Review Article

Nano Research
2023, 16(7): 9142–9157

ISSN 1998-0124 CN 11-5974/O4
https://doi.org/10.1007/s12274-023-5502-8

Electrocatalytic water splitting: Mechanism and electrocatalyst design

Han Wu[§], Qiaoxian Huang[§], Yuanyuan Shi, Jiangwei Chang (✉), and Siyu Lu (✉)

Green Catalysis Center, College of Chemistry, Zhengzhou University, Zhengzhou 450001, China
[§] *Han Wu and Qiaoxian Huang contributed equally to this work.*

Received: 17 December 2022 / **Revised:** 7 January 2023 / **Accepted:** 12 January 2023

ABSTRACT

Hydrogen energy, a new type of clean and efficient energy, has assumed precedence in decarbonizing and building a sustainable carbon-neutral economy. Recently, hydrogen production from water splitting has seen considerable advancements owing to its advantages such as zero carbon emissions, safety, and high product purity. To overcome the large energy barrier and high cost of water splitting, numerous efficient electrocatalysts have been designed and reported. However, various difficulties in promoting the industrialization of electrocatalytic water splitting remain. Further, as high-performance electrocatalysts that satisfy industrial requirements are urgently needed, a better understanding of water-splitting systems is required. In this paper, the latest progress in water electrolysis is reviewed, and experimental evidence from *in situ*/*operando* spectroscopic surveys and computational analyses is summarized to present a mechanistic understanding of hydrogen and oxygen evolution reactions. Furthermore, some promising strategies, including alloying, morphological engineering, interface construction, defect engineering, and strain engineering for designing and synthesizing electrocatalysts are highlighted. We believe that this review will provide a knowledge-guided design in fundamental science and further inspire technical engineering developments for constructing efficient electrocatalysts for water splitting.

KEYWORDS

water splitting, mechanism, *operando* spectroscopy, design strategy

1 Introduction

Critical challenges arising from environmental issues and the increasing consumption of fossil fuels have necessitated the development of high-efficiency, green, and sustainable energy technologies [1]. Renewable energy resources, including solar, wind, and geothermal energies, are alternatives to traditional fossil fuels [2]. However, the spatial distribution of these energy resources has severely limited their large-scale applications. Hydrogen energy is considered as an ideal substitute owing to its widespread sources, high calorific values of combustion, and zero carbon emissions. Currently, approximately 95% of the world's hydrogen is produced by the conversion of natural gas and fossil fuels. Additionally, the production process is energy-intensive, and the produced hydrogen is prone to contamination [3]. Conversely, electrocatalytic water splitting is a simple, safe, and high-purity process for hydrogen production and has attracted considerable attention in recent years [4].

Water splitting comprises a cathodic hydrogen evolution reaction (HER) and an anodic oxygen evolution reaction (OER). In recent years, abundant studies have focused on exploring the mechanism of water splitting on electrocatalyst surfaces, especially OER. The mechanism of OER can be mainly divided into the adsorption evolution mechanism (AEM), oxidation path mechanism (OPM), and lattice oxygen-mediated mechanism (LOM). Compared to the HER, which is a two-electron process, the OER is a four-electron process involving multiple sub-reactions, which leads to a high energy barrier and low energy conversion efficiency for water electrolysis [5]. Over recent decades, significant efforts have been devoted toward optimizing water-splitting systems and developing efficient HER/OER electrocatalysts. Various materials with high activities and selectivities, including noble metals, oxides/hydroxides, sulfides, and phosphates [6–8], have been developed. Among them, noble metal-based electrocatalysts (e.g., ruthenium, platinum, and iridium) and the corresponding oxides are excellent electrocatalysts for the HER and OER [9, 10], respectively. However, their limited reserves and high price have significantly limited their widespread application. To reduce the amount of noble metals while maintaining the excellent activity of these electrocatalysts, some effective strategies, such as reducing the particle size or nanocrystallization, alloying, and constructing heterogeneous interfaces, have been successfully developed, and the composition and electronic structures have been finely regulated such that a sufficient number of active sites are exposed for water splitting. Consequently, these materials exhibit immense potential to replace commercial electrocatalysts under experimental conditions [11–13]. However, when subjected to industrial conditions, these as-designed electrocatalysts have to withstand high currents and long running times, which requires the materials to simultaneously possess excellent activities and good corrosion resistances. Therefore, an atomic-level in-depth study of the water-splitting process has become an important topic

Address correspondence to Jiangwei Chang, jwchang2021@zzu.edu.cn; Siyu Lu, sylu2013@zzu.edu.cn

in recent decades [14–16]. Using advanced *in situ*/*operando* characterization techniques, including Raman/infrared spectroscopy and X-ray absorption fine structure analyses combined with theoretical predictions, researchers have realized the real-time tracking and monitoring of intermediates at a molecular level during water splitting [17–20]. Understanding the microscopic processes occurring on the electrocatalyst surfaces during water splitting is conducive toward establishing the intrinsic structure–activity relationship and providing important guidelines to design and develop highly efficient HER/OER electrocatalysts.

In this paper, the development of water splitting technology, HER and OER mechanisms, and design strategies for efficient electrocatalysts reported recently are introduced, as illustrated in Fig. 1. Experimental evidence from spectroscopic investigations combined with theoretical studies is summarized and analyzed in detail to present a mechanistic understanding. More importantly, some promising strategies developed to construct active sites and regulate electronic properties, such as the alloying and engineering of morphologies, interfaces, and defects, are discussed, and the corresponding structure–property relationships are established to enhance the catalytic efficiency of water splitting. Finally, this review provides a detailed summary of the problems and challenges regarding the future development of water-splitting technologies, with the aim of providing valuable insights into fundamental study and technical engineering for the optimal design and modification of highly efficient HER/OER electrocatalysts.

2 Reaction mechanism of water splitting

Water splitting is a simple and rapid process that can be performed at room temperature ($2H_2O + \text{energy} \rightarrow 2H_2 + O_2$). Specifically, positive and negative electrodes are inserted into an aqueous solution and connected to a power supply, and a certain voltage is applied to overcome the energy barrier required for the catalytic splitting of water molecules. Generally, hydrogen ions in an aqueous solution undergo a reduction reaction at the cathode to form H_2, whereas hydroxide ions undergo an oxidation reaction at the anode to form O_2. During this process, the change in the free energy (ΔG) of water electrolysis is 237.2 kJ·mol^{-1} at 25 °C and 1 atm with a theoretical voltage of 1.23 V to initiate water splitting. However, owing to the poor kinetics of the electrochemical reaction, a high overpotential is required to compensate the potential loss. Therefore, the water-splitting process often uses highly active electrocatalysts to facilitate electrochemical reactions on electrode surfaces to reduce energy consumption. Successful commercial applications of water electrolyzers, which are regarded as the next-generation renewable energy devices for the conversion of intermittent electricity generated from sustainable wind, solar, and tidal power into fuels [21, 22], are of great significance for addressing environmental issues and the energy crisis. Based on the different membrane materials in electrolytic cells, water splitting can selectively occur via proton exchange membrane, basic, or solid oxide electrolysis. In general, the HER and OER during energy conversion/storage play pivotal roles in improving the overall efficiency of water electrolysis. Therefore, knowledge-guided principles are needed to design optimal electrocatalysts with satisfactory activity, selectivity, and electrochemical stability for a particular reaction.

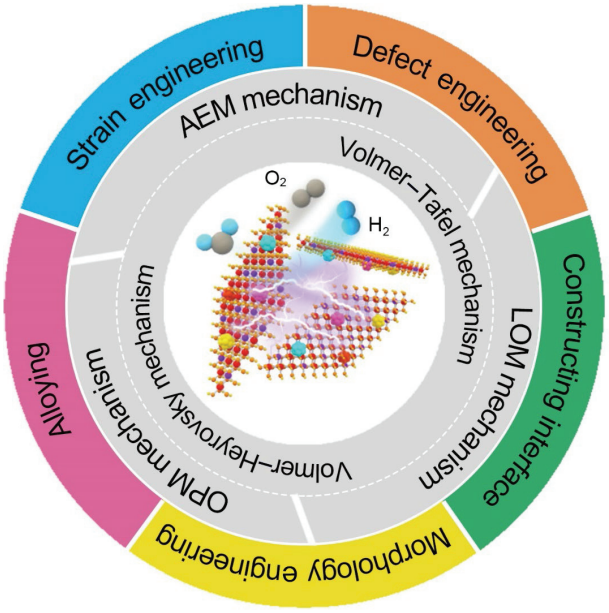

Figure 1 Mechanism of water splitting and electrocatalyst design strategies.

2.1 HER mechanism

The HER is a two-electron transfer process that occurs at the cathode surface to produce a hydrogen molecule. During this process, the electrical energy is converted into chemical energy. Although the mechanism of the HER is slightly different under acidic and alkaline conditions, both involve the adsorption and desorption of some typical reaction intermediates. As shown in Figs. 2(a) and 2(b), a proton is first adsorbed on the catalyst surface to form an adsorbed hydrogen intermediate (M-H_{ads}, where M represents the active site), which is accompanied by the deduction of one electron according to the Volmer reaction. The second step can be divided into the Tafel and Heyrovsky reactions, depending on the coverage of H_{ads}. These two reaction routes can be approximately identified using the Tafel slopes, which are calculated from the experimental plots of the overpotential as a function of log|current density|. Theoretically, the Tafel reaction refers to the direct coupling of two adsorbed hydrogens on an electrocatalyst surface to generate a hydrogen molecule, whereas the Heyrovsky reaction involves the combination of one adsorbed hydrogen on the electrocatalyst surface with another hydrogen ion in the electrolyte under acidic conditions, or another water molecule under alkaline conditions, to form a hydrogen molecule. Because the adsorbed hydrogen intermediate exists in both, the Volmer–Heyrovsky and Volmer–Tafel pathways, the free energy of hydrogen adsorption (ΔG_{Hads}) can serve as an important indicator reflecting the HER activity of electrocatalysts. According to the Sabatier principle, the ΔG_{Hads} of an ideal electrocatalyst should be close to zero. When ΔG_{Hads} is below zero, the bonding strength is too low to effectively activate the hydrogen adsorption reaction, resulting in a limited HER activity. In addition, ΔG_{Hads} values above zero are not ideal because the strong binding suggests difficult desorption of the M-H_{ads} intermediates, which correspondingly limits the total catalytic efficiency. Figure 2(c) shows a volcanic diagram of the HER activity and theoretical ΔG_{Hads} for different metal active sites [23]. Noble metals, such as platinum, have a ΔG_{Hads} close to zero and show high HER activity. Furthermore, ΔG_{Hads} can be adjusted close to zero by modifying the geometry and electronic structures of the active site, thus improving the hydrogen evolution activity. For example, to explore the relationship between the HER activity and thermodynamic ΔG_{Hads}, Lee et al. synthesized a series of silicon nanowire-supported metal electrocatalysts (metal/SiNWs) with modified metal–silicon interfaces [24]. Density functional theory (DFT) calculations showed that the constructed silicon–osmium interface performed best and exhibited an optimal ΔG_{Hads} of only −0.03 eV, far lower than those of monomeric osmium (−0.26 eV) and the noble metal platinum (−0.09 eV). Further tests also

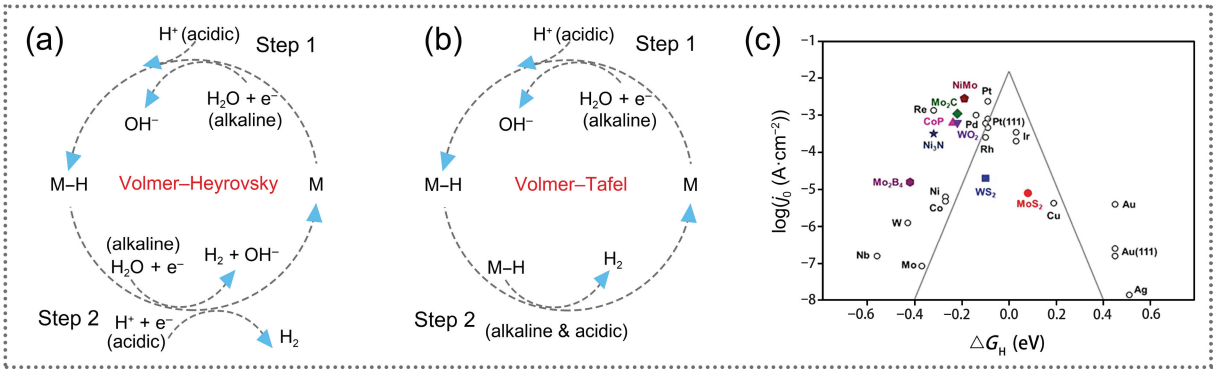

Figure 2 Reported HER mechanisms: (a) Volmer–Heyrovsky and (b) Volmer–Tafel pathways. (c). The HER Volcano plot for various transition metals against the ΔG_{Hads}. Reproduced with permission from Ref. [23], © Elsevier Ltd. 2019.

confirmed that Os/SiNWs exhibited an HER activity superior to that of commercial Pt/C.

2.2 OER mechanism

Compared with the HER, the OER follows a multistep proton-coupled electron transfer process with various elementary reactions. Therefore, the OER is a relatively slow kinetic process, which is a key factor restricting the total efficiency of water splitting. Under standard conditions, the thermodynamic equilibrium potential of the OER is 1.23 V; however, in most cases, an additional potential, i.e., the overpotential, is needed because of some adverse kinetic factors in actual water electrolysis. The overpotential can be reduced by introducing suitable electrocatalysts. Thus, understanding the OER mechanism can be conducive for theoretically designing more efficient electrocatalysts to reduce the overpotential.

According to recent explorations, three main OER mechanisms, including AEM, OPM, and LOM, have been proposed. The specific reaction process is illustrated in Fig. 3. In the AEM pathway (Fig. 3(a)), the OER is a four-step electron transfer process involving several reaction intermediates (such as OH_{ads}, O_{ads}, OOH_{ads}, and O_{2ads}). Specifically, hydroxides (in alkaline electrolytes) or water molecules (in acidic electrolytes) are first adsorbed onto the active sites of electrocatalysts to form M-OH_{ads}. The pre-adsorbed M-OH_{ads} is then converted to M-O_{ads}, which further converts to M-OOH_{ads} species. Finally, O_2 can be generated by losing a proton and an electron from M-OOH_{ads} in an acidic environment or by a proton-coupled electron transfer of M-OOH* under the attack of OH^- in an alkaline environment. For the OER in alkaline and acidic electrolytes, the change in the free energy of the entire reaction is 4.92 eV, and the step with a high Gibbs free energy is considered as the rate-determining step (RDS) of the OER. Referring to other reported studies, the adsorption free energy difference between OOH_{ads} and OH_{ads} intermediates ($\Delta G_{OOHads} = \Delta G_{OHads} + 3.2 \pm 0.2$ eV) remains constant, and the scaling relationship indicates that the two intermediate steps (step 2: OH_{ads} deprotonation; step 3: OOH_{ads} formation) are the RDSs. The overpotential can be expressed as: $\eta OER = \max[(\Delta G_{Oads} - \Delta G_{OHads}), 3.2 \text{ eV} - (\Delta G_{Oads} - \Delta G_{OHads})]/e$. According to the Sabatier principle, the oxygen binding strength acts as a key indicator and reflects the volcano-like activity in the η_{OER} vs. $(\Delta G_{Oads} - \Delta G_{OHads})$ plot, as shown in Fig. 3(c) [25]. A minimum overpotential of approximately 0.37 V can be predicted for the OER at a current density of 10 mA·cm^{-2}. Breaking the energy relationship between OH_{ads} and OOH_{ads} is the key to obtaining a lower overpotential and improving activities. Based on this, many effective strategies, such as doping heteroatoms, introducing vacancies, strain engineering, and interface construction [26, 27], have been successfully developed. For example, Sun et al. synthesized $Ni(OH)_2$ nanoparticles (NPs) using a reflux method; Ir NPs were anchored to the $Ni(OH)_2$ NPs ($Ir/Ni(OH)_2$) with rich interfaces aided by polyol reduction [28]. The results showed that the overpotential of $Ir/Ni(OH)_2$ at a current density of 100 mA·cm^{-2} was 270 mV, which was lower than those of $Ni(OH)_2$ (437 mV) and Ir NPs (343 mV). Moreover, an overpotential of 224 mV was required to deliver a current density of 10 mA·cm^{-2}, which was significantly lower than the minimum theoretical overpotential of the OER under the AEM pathway, as discussed above. Further investigation showed that the synergistic effect at the interface between the locally reconstructed IrO_x and NiOOH sites breaks the scaling relationship between OH_{ads} and OOH_{ads}, resulting in a remarkable enhancement in the OER kinetics. Furthermore, strong electronic interactions between the Ir species and $Ni(OH)_2$ and the Ir–O–Ni bridge bonds stabilized the metastable Ir(V) species and accelerated the formation of O–O bonds during oxygen evolution, further increasing the OER activity.

Recently, the LOM originating from lattice oxygen redox chemistry has served as an alternative route to rationalize the reconstruction of active species. Herein, oxygen ligands are electrochemically activated and released from the lattice matrix of the electrocatalysts, resulting in a high intrinsic activity. To date, several LOM-based OER pathways with different active centers have been proposed. Specifically, for a single active center, the activated lattice oxygen on the electrocatalyst surface can directly serve as the reactive site (known as the oxygen-vacancy-site mechanism (OVSM), shown in Fig. 3(d)) and receive OH^- through nucleophilic attack to form M-O_{lat}-OH_{ads} species. Subsequently, the produced O_2 is desorbed from the electrocatalyst surface, and thus, an oxygen vacancy is generated and subsequently refilled by OH^-. Alternatively, surface reconstruction of the electrocatalysts also allows direct coupling of the activated lattice oxygen and *O intermediates, in a process known as the single-metal-site mechanism (SMSM), which is energetically conducive to the formation of high-valence metal cations (Fig. 3(e)). Moreover, a dual-metal-site mechanism (DMSM) has been proposed, wherein adjacent activated lattice oxygen atoms directly couple to form an M-$O_{lat}O_{lat}$-M motif, and the produced O_2 can be released from the O_{lat}-O_{lat} moiety which acts as peroxo-like species (Fig. 3(f)). The DMSM was reported in metal (oxy)hydroxides because of their structural flexibility. Generally, electrocatalysts following the LOM can easily overcome the thermodynamic relationship limitations in the case of AEMs and provide a higher oxygen evolution activity. However, the participation of activated lattice oxygen can also induce the formation of oxygen vacancies on the electrocatalyst surface, and the resulting unsaturated metal sites tend to dissolve in the electrolyte, thus reducing the stability of the electrocatalyst [29, 30]. In other words, the high activity of electrocatalysts through the LOM is achieved at the expense of the stability, which is not

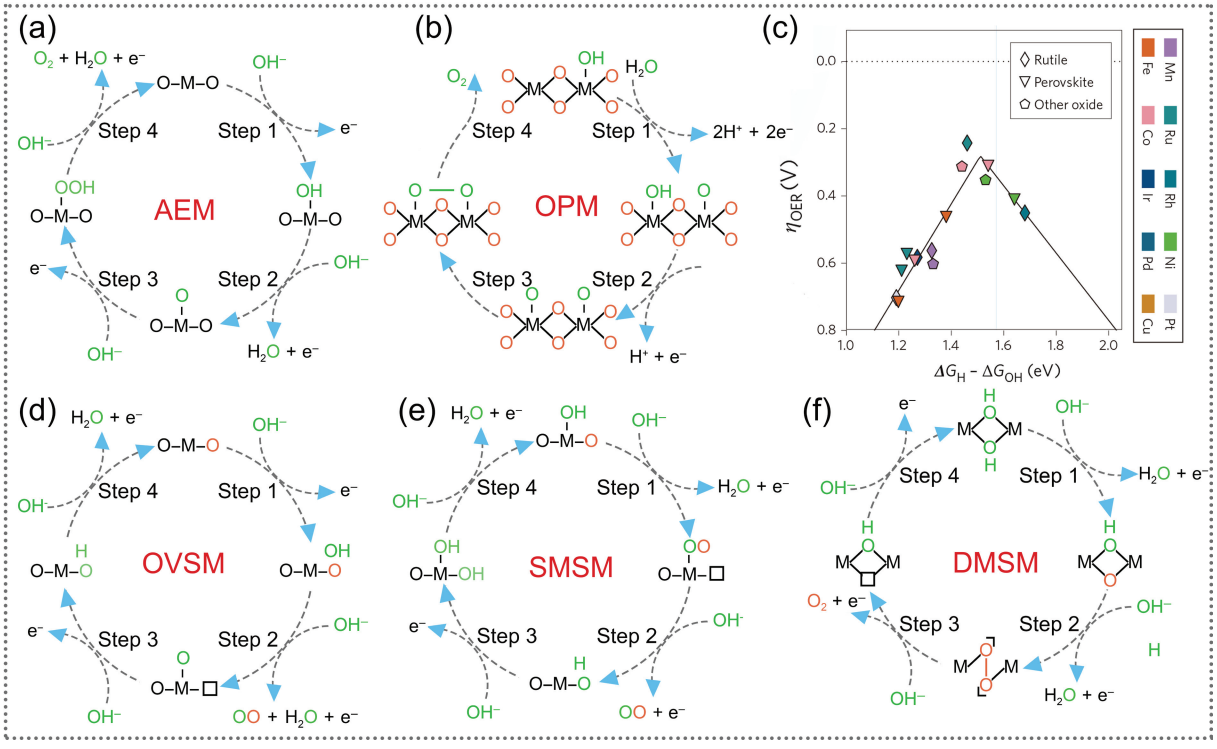

Figure 3 Reported OER mechanisms: (a) AEM, (b) OPM, and ((d)–(f)) LOM. (c) The volcano plot for various TMOs against the oxygen binding strength ($\Delta G_{Oads} - \Delta G_{OHads}$). Reproduced with permission from Ref. [25], © Nature Publishing Group, a division of Macmillan Publishers Limited. 2016.

beneficial for the development of electrocatalysts, particularly in acidic media. Ideally, heterogeneous electrocatalysts that operate through the OPM can effectively avoid this problem. Unlike the AEM and LOM, the OPM is more likely to enable the design of efficient OER electrocatalysts, where direct O_{ads}– O_{ads} radical coupling can be achieved without oxygen vacancies or additional reaction intermediates (e.g., OOH_{ads}) and only O_{ads} and OH_{ads} act as intermediates during the OER, as shown in Fig. 3(b). Specifically, two *OH groups are generated on two adjacent metal active centers via proton transfer from H_2O molecules in acidic media or the direct adsorption of OH^- from alkaline media. The two neighboring OH_{ads} are converted into two O_{ads} through two subsequent proton-coupled electron transfer steps, and O_{2ads} can be formed through a direct O_{ads}–O_{ads} radical coupling. Finally, O_{2ads} is desorbed from the surface. Under ideal conditions, polyphase electrocatalysts based on the OPM exhibit excellent activity and good stability. However, there are many stringent requirements for designing the geometry of a metal site that satisfies the OPM. Generally, symmetric dual-metal sites with appropriate atomic distances can accelerate the coupling of O_{ads}–O_{ads} radicals with a low energy barrier. Hu et al. described a unique iron-nickel oxide electrocatalyst, whose turnover frequencies (TOFs) under alkaline conditions were significantly higher than those of commercial $NiFeO_x$ electrocatalysts [31]. Theoretical calculations showed that compared with single-phase γ-NiOOH and γ-FeOOH, the iron-nickel oxide electrocatalyst had unique Fe and Ni dual active sites, where oxygen molecules could be directly formed through the nucleophilic attack of OH^-, thus greatly reducing the overpotential of the OER. Additionally, similar OER electrocatalysts in acidic media have been reported. Lee et al. reported an α-MnO_2 nanofiber-supported Ru composite (12Ru/MnO_2) that met the OPM design rules [32]. Small and regularly arranged chains of Ru atoms were generated, with Ru atoms replacing the surface Mn atoms by a cation exchange method (Fig. 4(a)). The results indicated that the Ru nanoarray in 12Ru/MnO_2 was composed of symmetrical Ru sites and the interatomic Ru–Ru distance (2.9 Å) was shorter than that in RuO_2 (3.1 Å), which is conducive to the O_{ads}–O_{ads} radical coupling. The *operando* synchrotron fourier transform infrared (FTIR) spectrum of 12Ru/MnO_2 shows that some enhancing absorption peaks assigned to O–O and metal–O–O bonds can be observed as the voltage increases, suggesting the forming oxygen bridges between metal sites in the OPM-type OER. In addition, the ^{32}O and ^{36}O signals were also detected by *operando* differential electrochemical mass spectrometry (DEMS) in the $H_2{}^{18}O$ and $H_2{}^{16}O$ electrolytes using 12Ru/MnO_2 as the electrocatalysts for OER, respectively, which further indicated that the OER in 12Ru/MnO_2 typically follows the OPM pathway. As a result, 12Ru/MnO_2 with a Ru loading of 11.6 wt.% required a low overpotential of only 161 mV to achieve a current density of 10 mA·cm^{-2}. Ru/MnO_2 also exhibited excellent long-term durability for more than 200 h and is one of the best acid-stable OER electrocatalysts reported to date.

The OER mechanism of an electrocatalyst is closely related to the intrinsic characteristics of active sites with a particular electronic structure. Generally, electrocatalytic oxygen evolution for metal oxides with good crystallinity and few defects tends to occur either through the AEM pathway with the generation of key OOH_{ads} intermediates at a single metal site or through the OPM pathway with O_{ads}–O_{ads} directly coupling at two adjacent metal sites. However, the LOM pathway tends to occur in amorphous metal oxides with abundant oxygen vacancies and perovskites with high metal–oxygen ligand covalency. For real applications of electrocatalysts, the determination of the OER pathway has great importance for decoupling the intrinsic activities of the electrocatalysts and optimizing the active sites toward better electrocatalytic performance. Various *in situ* characterization techniques, including *in situ* differential electrochemical mass spectrometry, FTIR spectroscopy, and Raman spectroscopy, and theoretical calculations have been used to capture and analyze the reaction intermediates or origin of the generated gas to further determine the oxygen evolution pathway [33–35]. Through a well-designed experiment in which Ir single atoms were selectively loaded onto the surface or into the lattice of CoOOH to obtain two kinds of structures (Ir_1/$CoOOH_{sur}$ and Ir_1/$CoOOH_{lat}$,

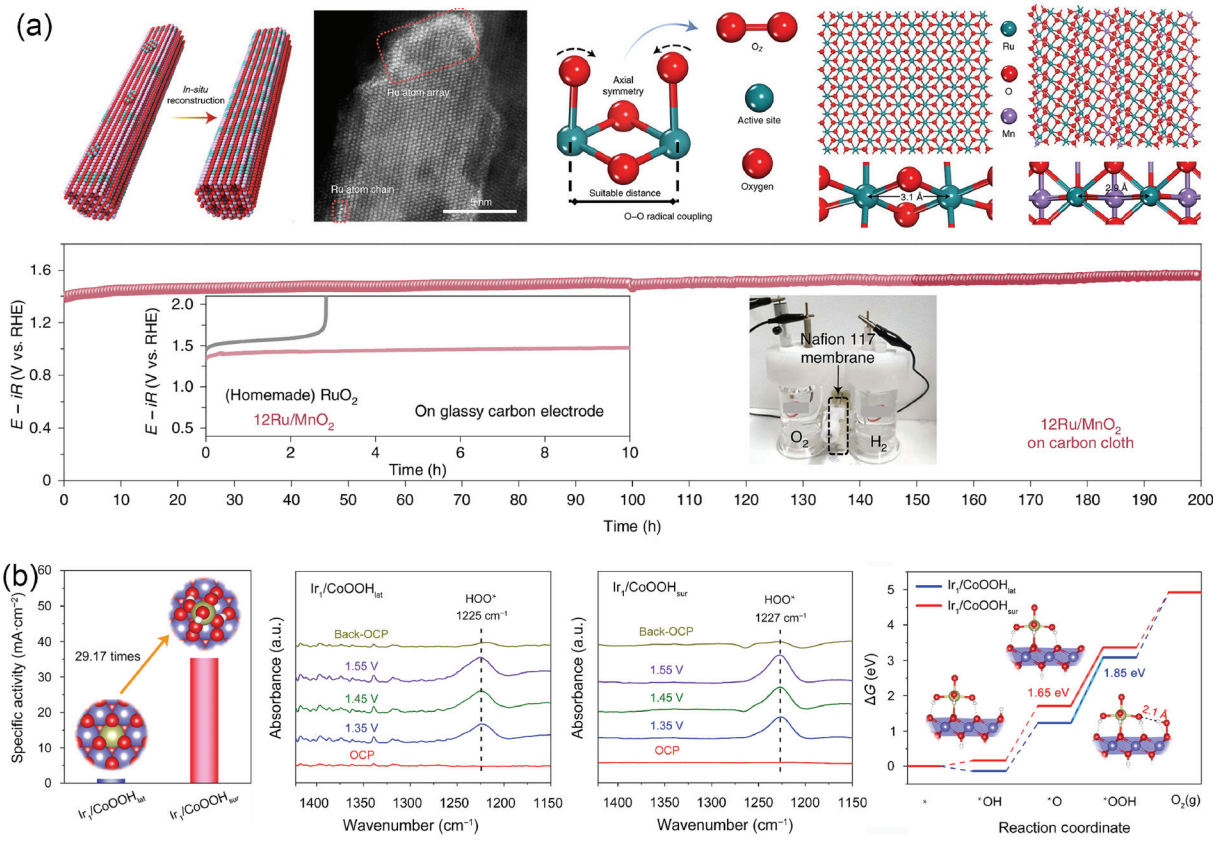

Figure 4 (a) Ru atom array on α-MnO_2 with enhanced performance for acidic water oxidation, and their structure and performance. Reproduced with permission from Ref. [32], © Lin, C. et al. 2021. (b) Iridium single atoms at different locations of CoOOH and their influences on oxygen evolution reaction: *in situ* FTIR spectroscopy and theoretical calculations. Reproduced with permission from Ref. [36], © American Chemical Society 2022.

respectively) with different OER activities [36], Zeng et al. thoroughly studied the influence of the location of the Ir active site on the OER mechanism using *in situ* FTIR spectroscopy combined with theoretical studies. As shown in Fig. 4(b), when the applied potential is gradually increased from the open-circuit potential to 1.35 V, notable peaks at approximately 1227 and 1225 cm^{-1}, representing O–O vibrations, are detected for $Ir_1/CoOOH_{sur}$ and $Ir_1/CoOOH_{lat}$, respectively. Additionally, the peaks disappear after the potential returns to the open-circuit potential, indicating that these peaks can be attributed to the emergence of OOH_{ads} intermediates during oxygen evolution. This validates that the oxygen evolution pathway of $Ir_1/CoOOH_{sur}$ and $Ir_1/CoOOH_{lat}$ follows a four-step AEM reaction, excluding the lattice oxygen-mediated O_{lat}–O_{lat} coupling pathway. Furthermore, the possible O_{ads}–O_{ads} coupling via the OPM was explored by DFT analysis at these two interfaces, and the resultant high theoretical overpotential suggested that the AEM pathway was more thermodynamically favored than the OPM. Finally, free energy diagrams of the AEM pathway for $Ir_1/CoOOH_{sur}$ and $Ir_1/CoOOH_{lat}$ were calculated for comparison. The energy barrier of the RDS (O_{ads} to OOH_{ads} transition) decreased from 2.09 (CoOOH) to 1.85 ($Ir_1/CoOOH_{lat}$) and to 1.65 eV ($Ir_1/CoOOH_{sur}$), indicating that the Ir atoms distributed on the surface of CoOOH could more effectively regulate the adsorption behaviors of intermediates than those in the lattice, which aptly explains the origin of the high OER activity for $Ir_1/CoOOH_{sur}$.

3 Strategies for optimizing electrocatalyst

Given the high energy barriers in water splitting, especially for the OER, numerous highly efficient electrocatalysts have been developed to accelerate water splitting and reduce energy consumption. Among them, noble metals (platinum, iridium, and ruthenium) and their oxides (iridium dioxide and ruthenium dioxide) are considered to be the best electrocatalysts for the HER and OER [37–39], respectively. However, various problems need to be resolved prior to practically applying these electrocatalysts. For example, pure noble metal-related electrocatalysts are prone to inactivation because of the inevitable agglomeration of active components during the reactions and the noble metal oxides tend to dissolve into the electrolyte because of excessive oxidation during oxygen evolution, especially in acidic media, thus reducing their electrocatalytic activities and stability [40, 41]. To resolve the aforementioned challenges faced by noble metal electrocatalysts and simultaneously enhance the activity of other non-noble metal electrocatalysts, some effective strategies have been proposed and successfully employed in the design and synthesis of electrocatalysts. Few representative electrocatalysts and their electrocatalytic performance for water splitting are listed in Tables S1 and S2 in the Electronic Supplementary Material (ESM).

3.1 Alloying

An alloy is typically composed of two or more metals. Compared with single metals, different metal atoms within an alloy usually exhibit strong interactions or synergies, which often result in better electrocatalytic performance [42–44]. Yao et al. synthesized a PtRu alloy with Pt and Ru dual sites using a facile laser irradiation strategy in a liquid [45], as shown in Fig. 5(a). The *in situ* X-ray absorption fine structure results show that the alloying degree of PtRu increases during electrocatalytic hydrogen evolution and that the alloying of Pt and Ru remarkedly regulates the hydrogen adsorption energy at the Pt site. Benefiting from these, the adsorption of hydroxyl on the Ru site is significantly improved, and the energy barrier for water dissociation is correspondingly reduced. Therefore, PtRu alloy NPs show excellent HER activities and stability in all pH ranges. Alloying

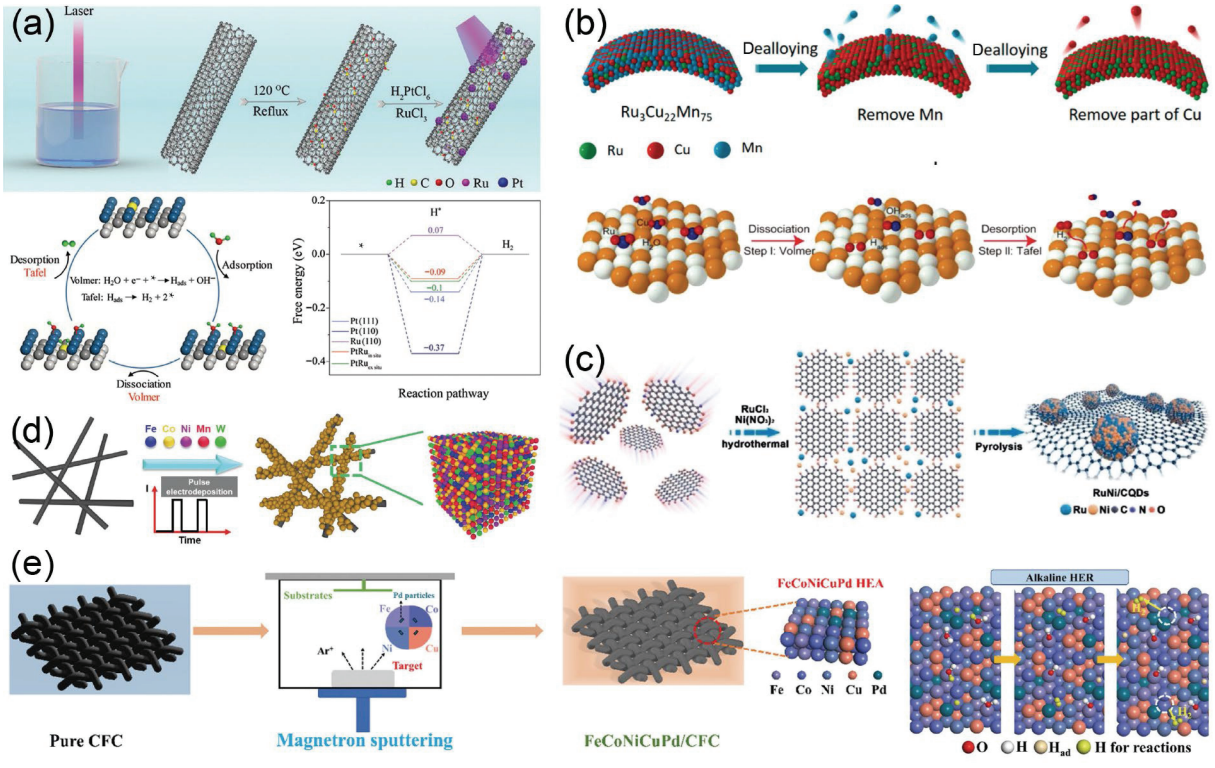

Figure 5 (a) The schematic illustration of the manufacture of the PtRu NPs on CNTs electrocatalyst and their alkaline HER mechanism. Reproduced with permission from Ref. [45], © The Royal Society of Chemistry 2022. (b) The schematic illustration of the preparation of the porous CuRu alloys and their alkaline HER mechanism. Reproduced with permission from Ref. [48], © American Chemical Society 2020. (c) The schematic illustration of the synthesis of the RuNi/CQDs electrocatalyst. Reproduced with permission from Ref. [51], © Wiley-VCH Verlag GmbH & Co. KGaA, Weinheim 2020. (d) Schematic illustration for fabrication of FeCoNiMnW. Reproduced with permission from from Ref. [54], © Elsevier B.V. 2022. (e) Schematic illustration of key FeCoNiCuPd thin film fabrication steps and the alkaline HER process. Reproduced with permission from Ref. [55], © Elsevier B.V. 2022.

between non-noble and noble metals is also a good approach to enhance the activity of non-noble metal electrocatalysts and simultaneously reduce the cost of noble metals [46, 47]. For example, copper is a poor electrocatalyst for the HER because of its low hydrogen-bonding energy. In contrast, ruthenium is the most widely used electrocatalyst for water splitting in alkaline media, but the interactions between Ru and H atoms are too strong, which will make it hard to desorb hydrogen. To overcome this, Tan et al. reported a three-dimensional porous CuRu alloy using a dealloying method [48], as shown in Fig. 5(b). The results showed that introducing Ru atoms into the Cu matrix can optimize the electronic interaction of Ru–H and accelerate the subsequent adsorption/desorption of intermediates during water splitting, which can significantly improve the HER efficiency in neutral and alkaline electrolytes. Pan et al. synthesized IrCo nanoalloys (IrCo NPs) with a low Ir content of 6.7 wt.% by directly calcinating binary metal-organic framework materials [49]. When tested in 0.5 M H_2SO_4, the IrCo NPs showed an outstanding catalytic activity for the HER and OER with only 23.9 and 270.0 mV overpotentials, respectively, to achieve a current density of 10 mA·cm^{-2}. Alessandri et al. synthesized a novel AuFe nanoalloy by laser ablation synthesis [50]. Owing to the highly loaded Fe atom (up to 11 at.%) in the Au lattice, the AuFe nanoalloy exhibited a high OER activity with an increase of up to 20 times the current density than the counterpart of pure metal NPs when measured in an alkaline aqueous solution. Lu et al. obtained a series of Ru-based bimetallic ultrafine nanocrystals (Ru–M, where M represents Ni, Mn, or Cu) using carbon quantum dots (CQDs) as the substrate to uniformly disperse metal ions and effectively induce the nucleation and growth of nanocrystals during pyrolysis (Fig. 5(c)) [51]. All these nanocrystals exhibit excellent HER activities much higher than that of the corresponding pure Ru nanocrystals at all pH levels. Specifically, the overpotentials of the as-designed RuNi/CQDs in 1.0 M KOH, 0.5 M H_2SO_4, and 1.0 M PBS were 13, 58, and 18 mV at a current density of 10 mA·cm^{-2}, respectively, when the loading of Ru was 5.93 mg_{Ru}·cm^{-2}. Theoretical studies demonstrated that the Ni atoms in the RuNi alloy can moderately modify the electronic environment of the adjacent Ru site to obtain an optimized hydrogen binding energy, thus improving the HER activity.

In recent years, high-entropy alloys (HEAs), a new type of nanoalloy material, have attracted wide interests in electrocatalysis because of their flexible compositions and high tolerance, especially in harsh testing environments. The selection of multiple components in HEAs can maximize the interatomic synergies and effectively optimize the electronic structure of alloys, thus decreasing the energy barrier of water electrolysis with enhanced activities [52, 53]. Lu et al. developed a pulsed electrodeposition method for the *in situ* growth of a high-entropy FeCoNiMnW alloy on the surface of carbon paper (Fig. 5(d)) [54]. Because of the unique advantage of atomic-scale synergies among multiple components in HEAs, FeCoNiMnW exhibited an ultra-low overpotential of 15 mV for the HER and an overpotential of 512 mV for the OER in 0.5 M H_2SO_4 at 10 mA·cm^{-2}. Furthermore, the assembled FeCoNiMnW//FeCoNiMnW couple can achieve the current density of 10 mA·cm^{-2} at a cell voltage of 1.76 V for overall water splitting and good operation stability for up to 6 d. Fang et al. prepared thin films of a high-entropy FeCoNiCuPd alloy with good crystallization by magnetron sputtering, as shown in Fig. 5(e) [55]. The FeCoNiCuPd film exhibited excellent activity for both the HER and OER. The electrolyzer fabricated using the FeCoNiCuPd films had a low cell voltage of 1.52 V to deliver the current density of 10 mA·cm^{-2} in 1.0 M KOH and maintained notable durability for more than 100 h at a high current of 800 mA·cm^{-2}, achieving efficient and stable alkaline water splitting.

The rich active sites and high-entropy cocktail effects in the FeCoNiCuPd film are conducive to accelerating the alkaline HER process. *In situ* structural characterization and electrochemical tests showed that the HEA surface was reconstructed during the OER process, and the formed (FeCoNi)OOH species further lowered the energy barrier of the RDS (O_{ads} → OOH_{ads}), thereby enhancing the OER performance.

3.2 Morphology engineering

The microstructure of a material has a significant influence on its physicochemical properties. Generally, the construction of highly open structures is helpful for enhancing the electrocatalytic performance [56]. A porous structure can not only promote the penetration and diffusion of the electrolyte into the electrocatalysts, thus ensuring that the reactants can adequately contact the active sites inside the bulk, but also provide more paths for charge and mass transport (including gas diffusion) during water splitting [57, 58]. In the last decade, material synthesis technologies have developed rapidly, and many effective strategies have been reported for regulating the microstructures of electrocatalysts. Among the various synthesis methods, there are two categories: directly regulating the active components and introducing foreign carriers with large surface areas and porous structures. The former is usually based on template-assisted methods, nanoarray construction, and surface etching methods during the synthesis process [59–61]. Qiao et al. directly grew $CoHPO_4$ nanoarrays on a highly conductive nickel foam through a low-temperature hydrothermal reaction, which further served as a sacrificial template in the subsequent potentiostat treatment for fabricating porous Co_3O_4 microtubule arrays (denoted as Co_3O_4-MTA), as shown in Fig. 6(a) [62]. The resultant unique structures enhanced mass and electron mobilities during hydrogen and oxygen evolution, achieving a high activity and stability. Furthermore, the as-constructed Co_3O_4-MTA materials were applied for overall water splitting as bifunctional electrodes and exhibited excellent performance comparable to that of commercial Pt/C and IrO_2/C electrodes. Yu et al. developed an ultrafast electrodeposition method to prepare a series of transition metal foams with three-dimensional porous structures for efficient water electrolysis (Fig. 6(b)) [63]. Benefiting from the *in situ* hydrogen bubble template generated during electrodeposition, the as-prepared metal foams had a unique three-dimensional channel for electrolyte diffusion and gas release and also exhibited high conductivity for facilitating fast interfacial charge transfer. Consequently, porous NiCo and NiFe foams can achieve good stability and outstanding activities for the HER and OER with only 86 and 206 mV, respectively, to deliver the current density of 10 mA·cm^{-2} in 1.0 M KOH. In addition, the assembled NiCo foam (–)//NiFe foam (+) electrolyzer only required 1.52 and 1.64 V to achieve the current density of 10 and 100 mA·cm^{-2}, respectively, significantly surpassing the Pt/C(–)//RuO_2(+)-based electrolyzer. Moreover, introducing appropriate carriers can also effectively regulate the microstructure or particle size of the electrode material to expose more reactive sites. Simultaneously, the rich porosity, good hydrophilicity, and large specific surface area of carriers can increase the accessibility of metal sites and improve the intrinsic activity of electrocatalysts [64, 65]. Lu et al. synthesized hydrophilic nitrogen-doped carbon quantum dots (NGQDs) using biomass ginkgo leaves as a source (Fig. 6(c)) [66]. Owing to their large surface areas and strong coordination with metal ions, NGQDs can effectively induce nucleation of Ru nanocrystals and further restrict their thermal agglomeration during pyrolysis. Ru nanocrystals (Ru@NGQDs) with an average size of 3.28 nm were thus obtained under optimal conditions. The

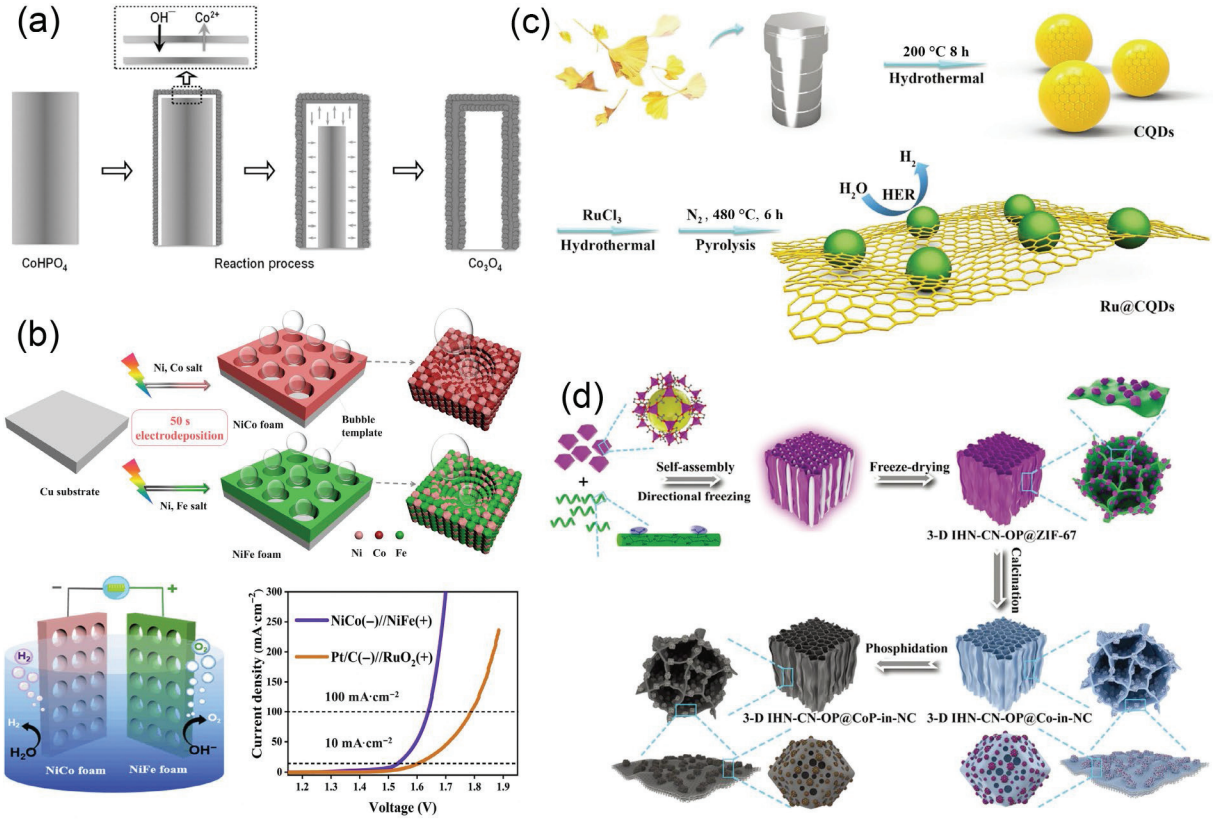

Figure 6 (a) Schematic illustration of the formation of Co_3O_4-MTA. Reproduced with permission from Ref. [62], © Wiley-VCH Verlag GmbH & Co. KGaA, Weinheim 2017. (b) Schematic diagram of the synthetic route of NiCo and NiFe foams and overall water splitting for two electrolyzers (NiCo foam and NiFe foam function as cathode and anode separately) in 1.0 M KOH. Reproduced with permission from Ref. [63], © Elsevier B.V. 2021. (c). The schematic illustration of the synthesis of the Ru@NCQDs electrocatalyst. Reproduced with permission from Ref. [66], ©. WILEY-VCH Verlag GmbH & Co. KGaA, Weinheim 2018. (d). The schematic illustration of the synthesis process of 3D IHN-CN-OP@CoP-in-NC. Reproduced with permission from Ref. [67], © Wiley-VCH GmbH 2021.

small size of Ru nanocrystals combined with the good hydrophilicity of NGQDs endowed the as-designed Ru@NGQDs with excellent electrocatalytic performance for the HER in 1.0 M KOH: The onset overpotential was 0 mV and an overpotential of only 10 mV was required to deliver the current density of 10 mA·cm^{-2} with good durability. In addition, Li et al. synthesized a three-dimensional carbon nanofiber-supported zeolite imidazole framework (ZIF-67) aerogel and converted it to three-dimensional CoP NP-embedded hierarchical N-doped carbon nanosheets (3D IHN-CN-OP@CoP-in-NC) via calcination and phosphatization (Fig. 6(d)) [67]. Electrochemical tests showed that 3D IHN-CN-OP@CoP-in-NC exhibited an outstanding HER activity at high current densities in both acidic and alkaline solutions, and the current remained stable after 2000 CV cycles or even after 20 h of chronoamperometric measurements, surpassing that of the commercial Pt/C electrocatalysts. The study showed that the high catalytic activity and fast reaction kinetics of 3D IHN-CN-OP@CoP-in-NC under high current densities were because of the three-dimensional interconnected carbon nanostructures in the bulk, which are conducive to fast electron transport, electrolyte penetration, and rapid release of hydrogen molecules within the electrocatalyst. Moreover, the highly dispersed CoP NPs embedded in the three-dimensional framework provided abundant electrochemically accessible active sites for the HER.

3.3 Interface engineering

Recently, rational design and development of abundant heterogeneous electrocatalysts have received extensive attention owing to their unique interfacial structures, where redistribution of electrons occurred, forming new chemical bonds and generating abundant active sites [68, 69]. Various types of electronic interactions at the interface have been proposed, such as the Mott–Schottky effect, electronic metal-support interactions (EMSIs), and support–stabilizing effect, among which, the Mott–Schottky effect is the most common. Owing to the thermal equilibrium and generation of two oppositely charged regions, the electronic density at the interface can be selectively changed, and thus the adsorption of reaction intermediates can be modified, ultimately accelerating the reaction kinetics of water splitting [70, 71]. Regulating d-orbital electrons of the active center based on the EMSI effect between the metal sites and carriers has been demonstrated to be effective for the further improvement of both the activity and durability of electrocatalysts [72]. Wang et al. constructed Pt-RuO_2@KB heterostructures with strong metal–carrier interactions [73]. Pt acted as a stable electron donor at the interfaces, and the electron transfer from the Pt to RuO_2 further gave rise to a stable charge redistribution around the interfaces, thus significantly reducing the energy barriers of water splitting. Moreover, owing to the strong electronic effects on stabilizing the Ru–O bond, oxygen vacancies in the bulk were significantly relieved because of the improved formation energy, which effectively inhibited the dissolution of active metal atoms into the acidic medium. Hence, Pt-RuO_2@KB exhibited an ultrahigh intrinsic activity and outstanding stability for the OER in 0.1 M $HClO_4$ electrolytes. Additionally, the reasonable construction of two-phase interfaces with two different active sites but complementary functions is an effective strategy to obtain high electrocatalytic performance based on intimate synergistic effects [74]. Wang et al. doped noble metal Pt into a Ni_4Mo alloy (denoted as Pt-Ni_4Mo) using a solvent-free microwave reduction method [75]. Electrochemical tests showed that the carbon nanotube (CNT)-supported Pt-Ni_4Mo exhibited excellent HER activity in alkaline electrolytes. Furthermore, *in situ* infrared absorption spectroscopy tests and DFT analysis showed that strong synergistic effects existed between the Pt and Ni_4Mo interfaces during hydrogen evolution and the Ni_4Mo site primarily dissociated water to produce H_{ads}, which was then transferred to the Pt active site, accelerating the H_2 desorption process. Shao et al. constructed a (Ni, Fe)S_2@MoS_2 heterostructure via hydrothermal synthesis using NiFe-LDH as the precursor. The (Ni, Fe)S_2@MoS_2 showed excellent activity, requiring low overpotentials of only 130 and 270 mV for the HER and OER, respectively, to obtain the current density of 10 mA·cm^{-2} and good durability for water splitting in an alkaline solution [76]. Moreover, *in situ* Raman spectroscopy further demonstrated that the as-designed interface is advantageous for the formation of stable S–H_{ads} and OH_{ads} intermediates to promote overall water splitting.

An in-depth understanding of the interfacial structure is essential for the optimal design and development of high-performance electrocatalysts. According to the structural features of materials, these interfaces mainly exist in supported, core–shell, and heterogeneous structures [59, 77, 78]. Peng et al. synthesized mesoporous Fe_2O_3/CuO heterostructures fixed on nickel foam using a template-free method [79], as shown in Fig. 7(a). The as-designed Fe_2O_3/CuO electrocatalysts with rich interfaces and Fe–O–Cu bridge bonds promoted the adsorption/desorption of oxygen-containing intermediates by enhancing the oxygen binding energy, which endows them with excellent performance and long-term durability in both the HER and OER. Additionally, single-atom materials are a new type of supported electrocatalyst owing to their nearly 100% atomic utilization and abundant atomic-scale interfaces with intrinsically different coordination structures [80–82]. Wang et al. reported Ni single atoms loaded on porous carbon nanofibers as HER electrocatalysts, where the chemical coordination structure of single-atom Ni was regulated by doping different heteroatoms, such as P, N, B, and S [83]. Studies have shown that introducing heteroatoms can polarize the charge distribution around Ni sites and adjust the electronic states toward the Fermi level, eventually leading to the optimal adsorption/desorption behavior for H/O-containing intermediates during water splitting. Based on the experimental and theoretical calculation results, the Ni atoms coordinated with one P and three N atoms were optimal to achieve outstanding electrocatalytic activity for water splitting. Furthermore, interfaces consisting of different crystalline phases have also been widely reported, providing new insights into the design of heterogeneous electrocatalytic materials [84, 85]. Fei et al. developed a core–shell-configured composite composed of an amorphous/crystalline phase NiFe alloy coated with ultrathin graphene layers (denoted as a/c-NiFe-G) using a microwave thermal-shock method [86], as shown in Fig. 7(b). The amorphous/crystal heterostructure generated abundant active sites, while graphene on the outside acted as a protective layer and electron transport pathway during water electrolysis, both of which resulted in a significantly improved OER performance. Therefore, the overpotential of a/c-NiFe-G at the current density of 10 mA·cm^{-2} was 250 mV in 1.0 M KOH, which was much lower than that of the corresponding graphene-layer-encapsulated crystalline phase NiFe alloys. Further, characterization methods such as X-ray absorption fine structure analysis combined with DFT calculations, also indicated that the abundant phase boundaries can effectively adjust electronic structures in the a/c-NiFe-G, leading to suitable adsorption energies for reaction intermediates, thereby enhancing the OER performance.

3.4 Defect engineering

Defects are common or inevitable in as-prepared electrocatalytic materials [87, 88], and various types of defects have been reported, including point (e.g., vacancy defects, heteroatomic substitution,

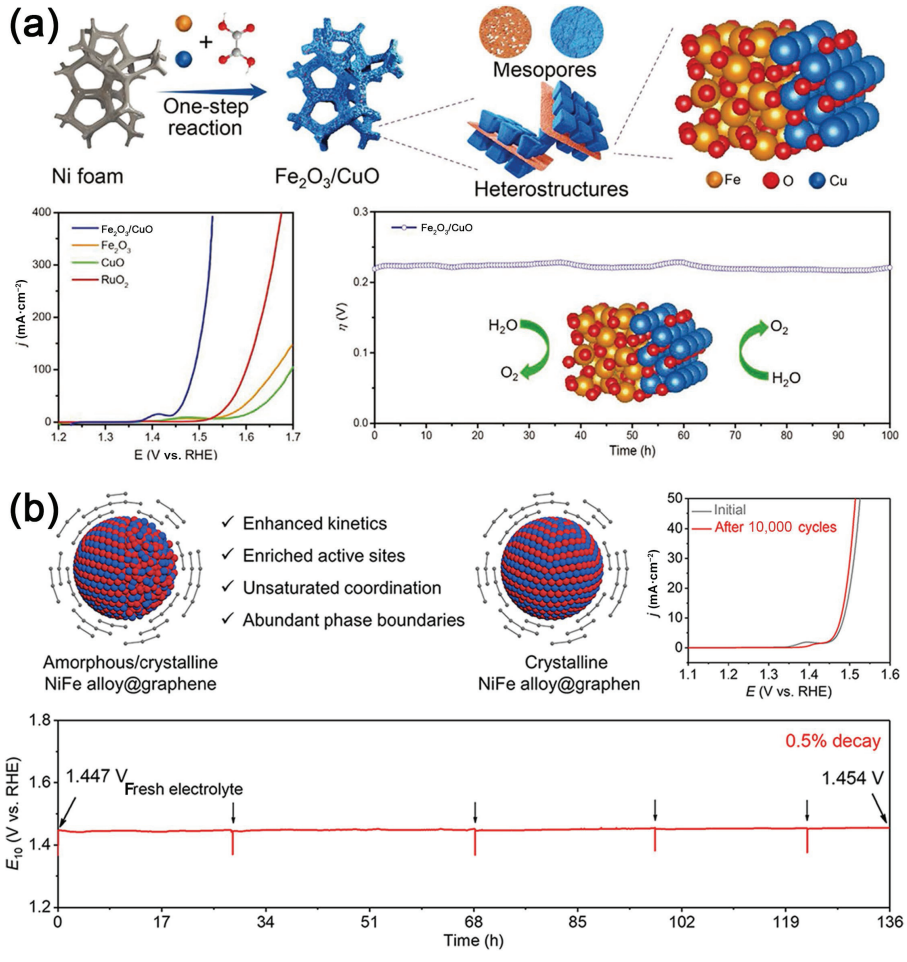

Figure 7 (a). Scheme illustrating the one-step growth of Fe_2O_3/CuO heterostructures on Ni foam and water splitting performance in 1.0 M KOH. Reproduced with permission from Ref. [79], © Wiley-VCH GmbH 2022. (b). The structural and compositional characterization of a/c-NiFe-G and c-NiFe-G and electrochemical OER performance in 1.0 M KOH. Reproduced with permission from Ref. [86], © American Chemical Society 2021.

and interstitial atoms), linear (e.g., edge dislocations), two-dimensional (e.g., crystal boundaries), and bulk defects (e.g., pores and foreign impurities) [89–92]. During electrocatalytic water splitting, the defects act as reactive centers as well as nucleation sites for constructing more active components. For example, the defect sites on the surface of substrates can capture and anchor metal species during material synthesis, thus achieving uniform dispersion and stabilization of metal-isolated sites in electrocatalysts [93]. To obtain high-density accessible active sites on the electrocatalyst surface, Liu et al. applied cobalt-doped ZIF-8-derived porous carbon (denoted as Co_1NC) for adsorbing a platinum precursor (chloroplatinic acid) and subjected it to a mild electrochemical reduction condition to prepare nitrogen-doped porous carbon materials with atomically dispersed Pt and Co (denoted as Pt_1/Co_1NC) [94]. As shown in Fig. 8(a), the abundant defects on the surface of Co_1NC play an important role in anchoring and dispersing Pt species toward forming atomically distributed Pt–N/C sites. The results showed that the Pt_1/Co_1NC exhibited excellent HER activity with a low overpotential of 4.15 mV to reach the current density of 10 mA·cm^{-2} with good stability for 5000 CV cycles. Xie et al. demonstrated that the introduction of defects into MoS_2 nanosheets (denoted as DR-MoS_2) activated the basal planes and generated abundant additional active sites for the HER. DR-MoS_2 had large surface areas exposing abundant defects, which can also provide abundant reaction sites for the adsorption and anchoring of Pt atoms, leading to uniformly dispersed Pt nanocrystals on DR-MoS_2 (denoted as DR-MoS_2-Pt) [95]. Benefiting from the strong synergy between the Pt nanocrystals and DR-MoS_2, the DR-MoS_2-Pt electrocatalyst showed excellent HER performance, better than the Pt/C electrocatalyst under both acidic and alkaline conditions. Wang et al. adopted electrochemical exfoliation to prepare double-transition-metal MXene nanosheets with abundant surface Mo vacancies (denoted as $Mo_2TiC_2T_x$-V_{Mo}) that were utilized to anchor single Pt atoms (designated as $Mo_2TiC_2T_x$-Pt_{SA}), as shown in Fig. 8(b) [96]. During the electrochemical exfoliation process, where $Mo_2TiC_2T_x$ deposited on carbon paper acted as a working electrode and Pt foil was adopted as a counter electrode, the Mo vacancies were refilled by Pt single atoms, and the Pt–C covalent bonds were reconstructed on the MXene surface. The as-synthesized $Mo_2TiC_2T_x$-Pt_{SA} electrocatalyst exhibited excellent kinetics for the HER with outstanding overpotentials of 30 and 77 mV for 10 and 100 mA·cm^{-2}, respectively, and remarkable stability of up to 10,000 cycles or 100 h of testing. Furthermore, the introduction of defects can also greatly regulate the local electronic structure to generate strong synergistic effects and form extra active sites [97–99]. To date, various strategies for defect engineering have been used for the surface modification of electrocatalysts, such as high-temperature reduction, plasma treatment, surface etching, and chemical reduction [100–102]. Because perturbations of the electron/charge distribution at a nanoscale are more pronounced than those at a macroscale, significant impacts of defects at the nanoscale on the physicochemical properties of electrocatalysts can be expected. Dai et al. treated Co_3O_4 nanosheets using an argon-plasma etching strategy; the obtained Co_3O_4 nanosheets possessed a large surface area, where abundant oxygen vacancies and Co^{2+} were generated [103] (Fig. 8(c)). The oxygen vacancies on the surface enhanced

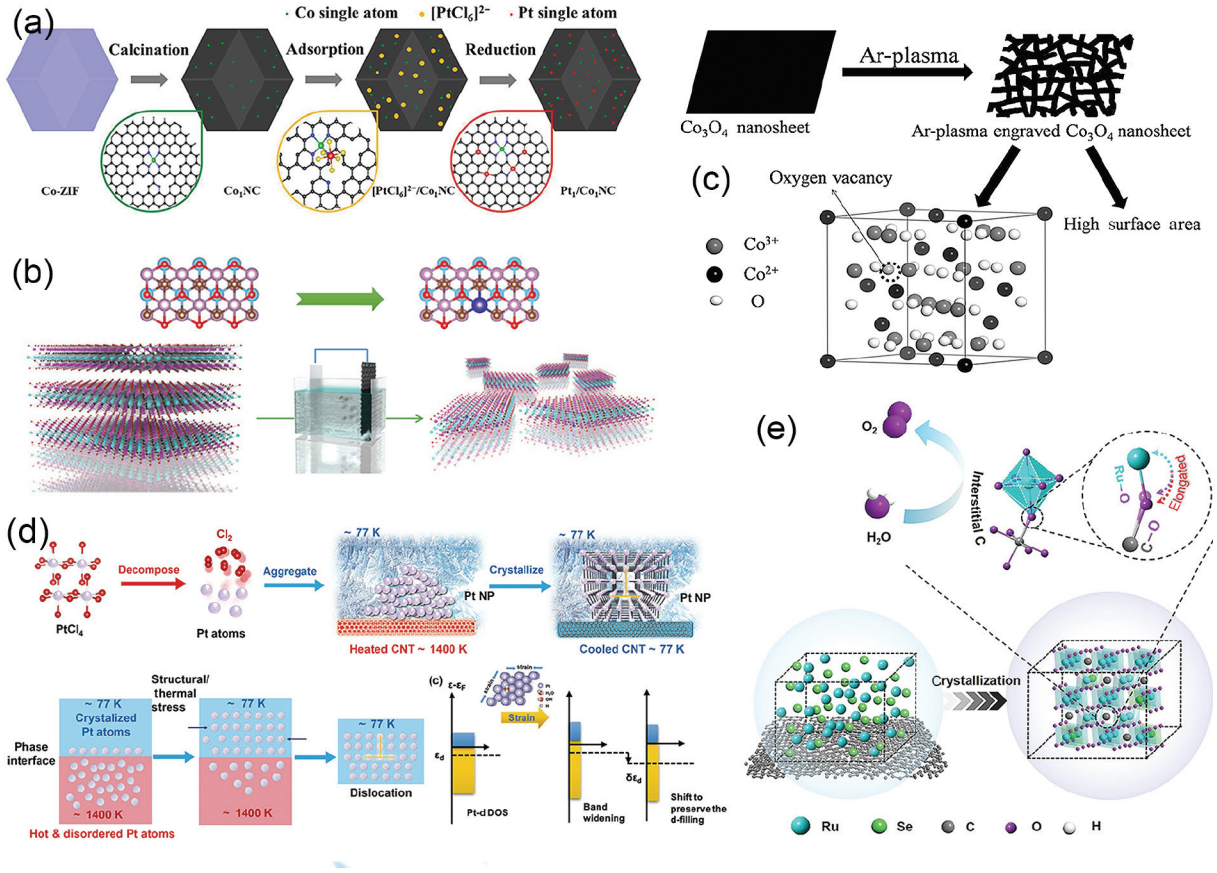

Figure 8 (a) The scheme illustrates the preparation of Pt_1/Co_1NC. Reproduced with permission from Ref. [94], © Elsevier B.V. 2021. (b). The schematic of the electrochemical exfoliation process of MXene with immobilized single Pt atoms. Reproduced with permission from Ref. [96], © Zhang, J. Q. et al. 2018. (c). The illustration of the preparation of the Ar-plasma-engraved Co_3O_4. Reproduced with permission from Ref. [103], © WILEY-VCH Verlag GmbH & Co. KGaA, Weinheim 2016. (d). Schematic diagram of the preparation of dislocation-rich Pt nanoparticles by environmental high-temperature thermal-shock. Reproduced with permission from Ref. [104], © Wiley-VCH GmbH 2021. (e) The formation process of C-RuO_2-RuSe. Reproduced with permission from Ref. [108], © Elsevier Inc. 2022.

the electronic conductivity of Co_3O_4, and highly exposed surface of Co_3O_4 provided more active sites for the OER. Compared with the pristine Co_3O_4, the etched Co_3O_4 showed a higher specific activity and current density at the same voltage. Chen et al. proposed a simple high-temperature thermal-shock strategy, followed by rapid cooling using liquid nitrogen, to introduce abundant dislocations into Pt NPs (denoted as Dr-Pt) [104], as shown in Fig. 8(d). The results showed that these dislocations induced a strong strain effect, which effectively modulated the electronic structure of Dr-Pt and optimized its catalytic HER activity. Dr-Pt possessed a low overpotential of 25 mV at 10 mA·cm^{-2} in a 1.0 M KOH electrolyte with good electrocatalytic stability for 20 h of testing. Recently, heteroatom doping has been regarded as a simple and efficient method to introduce defects and enhance the intrinsic activity of electrocatalysts [105–107]. Huang et al. demonstrated that the existence of interstitial carbon in the lattice of ruthenium dioxide (C-RuO_2-RuSe) can enhance its stability and activity for the OER in acidic media. The C-RuO_2-RuSe electrocatalyst was successfully obtained by pyrolyzing a carbon-supported $RuSe_2$ precursor, in which a large amount of free space was generated for rapid penetration and fixation of carbon atoms in the RuO_2 lattice gaps [108], as shown in Fig. 8(e). Compared with commercial RuO_2, the synthesized C-RuO_2-RuSe showed enhanced OER activity and excellent stability in 0.5 M H_2SO_4. Both experimental and theoretical results showed that the activation of Ru sites by interstitial C can optimize the reaction energy barrier toward enhanced activity and the interstitial C can also weaken the Ru–O bond covalency to effectively inhibit Ru dissolution, thus significantly improving its stability. Lu et al. reported CD-loaded molybdenum phosphide composites (MoP/NCDs) with different N-doping amounts [109]. In 1.0 M KOH, the MoP/NCDs delivered the current density of 10 mA·cm^{-2} under an overpotential of only 70 mV. DFT calculations further revealed that the incorporation of N atoms can function as promoters to reduce the ΔG_{Hads} of the MoP/NCDs; specifically, ΔG_{Hads} was effectively decreased by increasing the N-doping content. By optimizing the N-doping content, the electronic arrangement and charge density around the MoP active sites can be modified to promote the adsorption of HER intermediates.

3.5 Strain engineering

Strain engineering provides a new strategy for optimizing the geometric configuration and electronic structures of electrocatalysts and improving their HER/OER performance [110, 111]. Based on the relative direction of external forces applied to the stress region, the elastic strain can be classified as tensile, compressive, and shear strain. For electrocatalysts, the d-band center of the metal site is important because the electronic interactions originating from the orbital hybridization between the adsorbate and metal center are the key factors influencing the adsorption/desorption behavior. Elastic lattice strain can be used to adjust the Fermi level of the metal site, where small changes in the environment can significantly change the d-band states of the metal and its interactions with the adsorbate states [112, 113]. Hong et al. successfully introduced in-plane strain into noble metal nanosheets by constructing rich amorphous crystalline phase boundaries [114]. As shown in Fig. 9(a), for the

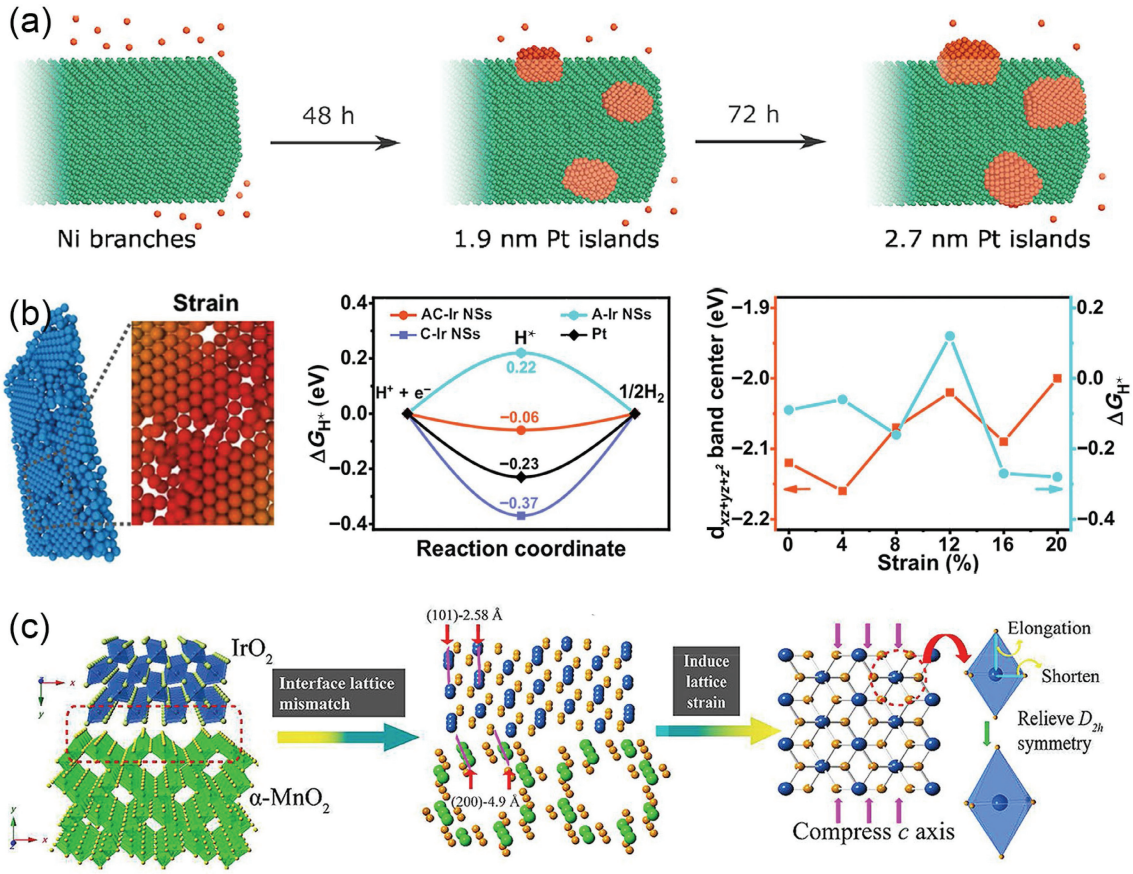

Figure 9 (a) The in-plane strain engineering through constructing amorphous-crystalline phase boundaries and the calculated ΔG_{Hads} and d-band centers on AC-Ir NSs. Reproduced with permission from Ref. [114], © Wu, G. et al. 2022, Ref. [121], © American Chemical Society 2019. (b) The scheme illustration growth of Pt atoms directly on a Ni branch. (c) The diagram process of α-MnO_2 substrate inducing the lattice strain of IrO_2. Reproduced with permission from Ref. [122], © American Chemical Society 2017.

as-synthesized ultrathin amorphous-crystalline Ir nanosheets (AC-Ir NSs), approximately 4% of the compressive strain was observed owing to the difference in the lattice constants in the local amorphous/crystalline boundary. DFT calculations confirmed that tensile strain can effectively adjust the d-band states of AC-Ir NSs, thereby optimizing the hydrogen adsorption energy and improving the HER performance. The TOF of the AC-Ir NSs was 4.5 times higher than that of the Pt/C electrocatalyst in the reference. Lu et al. reported a cobalt-ruthenium nanoalloy supported by CQDs (CoRu/CQDs) as an electrocatalyst for hydrogen evolution [115]. The introduction of a small amount of Ru (1.33 wt.%) into the cobalt crystal produced tensile strain in the CoRu alloy NPs and further accelerated the electron transport dynamics during the HER. Simultaneously, the introduction of Ru greatly regulated the electronic structure of Co, and thus, the electroactivity and adsorption strength of H_{ads} intermediates reached a perfect harmony, delivering efficient HER catalytic activities. Transition metal sulfides, such as molybdenum disulfide, can also be modified by introducing sulfur vacancies, thus inducing strain on the inert surface to enhance its electrocatalytic hydrogen evolution performance [116, 117]. Therefore, constructing compressive strain can effectively improve the activity of metal-based electrocatalysts by optimizing the adsorption capacity of the catalytic sites for the reaction intermediates. To date, many mechanisms based on lattice mismatch, morphology modulation, and substrate control [118–120] have been reported to introduce lattice strains. Lattice mismatch usually occurs at crystal interfaces with different lattice parameters and its effects on the structures of electrocatalysts have been widely explored. This mismatch can lead to strain at the edges of crystal frameworks, heterostructures, or defect sites, thus optimizing the adsorption strength of reaction intermediates and, eventually, improving electrocatalytic activities. Tilley et al. reported Pt islands grew directly on Ni NPs via slow reduction synthesis [121], as shown in Fig. 9(b), in which the strain content could be controlled by adjusting the size of the Pt islands. The study demonstrated that strain can affect the H-adsorption/desorption ability, and the strained Ni-branched Pt-island NPs had weaker hydrogen binding energy than that of commercial Pt, which led to faster H_2 desorption and thus, increased TOF during electrocatalysis. Yang et al. reported the construction of lattice strains by growing IrO_2 NPs directly onto the selectively exposed (200) crystal face of α-MnO_2 nanorods via continuous hydrothermal synthesis, as shown in Fig. 9(c) [122]. Interestingly, the OER activity of the prepared hybrid increased when the mass of IrO_2 decreased. Experimental results combined with theoretical calculations demonstrated that lattice mismatches at the underlying interface induced lattice strain in IrO_2. More importantly, the trend of lattice strain variation of IrO_2 NPs was consistent with their electrocatalytic activities, thus verifying the key role of the lattice strain in determining the OER activity.

4 Summary and outlook

In this paper, recent developments in this field are reviewed in detail, focusing on the mechanisms of water splitting, including hydrogen and oxygen evolution. The development of electrocatalysts is summarized, and some representative strategies for the design and synthesis of electrocatalysts, such as alloying, morphological engineering, interface construction, defect engineering, and strain engineering, are described. Although great progress has been made in developing efficient water-splitting

electrocatalysts and numerous studies have been reported in recent years, many difficulties remain to be urgently resolved to promote the industrial applications of electrolytic water splitting.

Firstly, the stability of electrocatalysts, especially at high current densities and under rigorous electrolyte environments, is of great significance for the practical application of water-splitting systems. Long-term and stable operation under a high current density is a substantial requirement for electrocatalysts, which requires high structural strength and excellent corrosion resistance. However, most of the stability evaluations of electrocatalysts for water splitting were performed at current densities of less than 1000 mA·cm^{-2} and exhibited poor durability, for example, less than one week or a much shorter time, which is not beneficial for the design and development of high-performance electrocatalysts. Additionally, the traditional electrode preparation process of fixing powders on the electrode surface using a binder may not be suitable, because rapid bubble desorption under high currents causes the peeling off of these active components and reduces the hydrogen evolution performance. Therefore, the development of binder-free self-supporting electrocatalysts is necessary.

Secondly, reducing the consumption of electrical energy and manufacturing cost of electrocatalysts is conducive toward reducing the cost of hydrogen production. The reduction in energy consumption in water splitting can be achieved by reducing the overall voltage of electrolyzers under the same current density. Owing to the slow kinetics of the OER, it is important to develop efficient oxygen evolution electrocatalysts and particularly, bifunctional electrocatalysts. However, oxidation reactions at low potentials (such as urea oxidation) have been widely reported to replace the anodic OER, reducing the overall voltage of water splitting. Therefore, substantial advancements are needed for the rational design and preparation of efficient redox media to facilitate the development of water splitting technology.

Finally, elucidating the structure–activity relationship can provide in-depth insights into the design and development of powerful HER/OER electrocatalysts aimed at the commercial application of water electrolyzers. Thus far, *in situ* characterization techniques, such as *in situ* FTIR spectroscopy, Raman spectroscopy, and DEMS, have been applied to reveal the electrocatalytic mechanisms of water splitting. Nevertheless, during actual water electrolysis, the active sites of the electrocatalysts are often reconstructed by the continual adsorption/desorption steps of the key intermediates and the dynamic changes in the interface between the electrocatalyst and the electrolyte, which makes it difficult to track a specific reaction species on the electrocatalyst surface and identify the real active sites. Hence, spectroscopic techniques with atomic resolutions and sensitivity remain in demand. *Operando* X-ray absorption spectroscopy is regarded as an effective tool for identifying the local coordination and electronic structures of the electrocatalysts during water splitting. Theoretical studies that use simplified models to analyze complex reaction processes may not be able to simulate real catalyst structures and chemical reactions. Therefore, a new calculation method involving more accurate models at a (semi-)quantitative level is required to effectively guide the design of electrocatalysts.

Acknowledgements

This work was partly supported by the National Natural Science Foundation of China (Nos. 52202050, 52122308, 21905253, and 51973200), the China Postdoctoral Science Foundation (No. 2022TQ0286), and the Natural Science Foundation of Henan Province (No. 202300410372).

Electronic Supplementary Material: Supplementary material (some representative electrocatalysts and their electrocatalytic performance for water splitting, and Tabs. S1 and S2) is available in the online version of this article at https://doi.org/10.1007/s12274-023-5502-8.

References

[1] Chu, S.; Majumdar, A. Opportunities and challenges for a sustainable energy future. *Nature* **2012**, *488*, 294–303.

[2] Rahman, A.; Farrok, O.; Haque, M. Environmental impact of renewable energy source based electrical power plants: Solar, wind, hydroelectric, biomass, geothermal, tidal, ocean, and osmotic. *Renewable Sustainable Energy Rev.* **2022**, *161*, 112279.

[3] Wu, H.; Cheng, Y. J.; Wang, B. Y.; Wang, Y.; Wu, M.; Li, W. D.; Liu, B. Z.; Lu, S. Y. Carbon dots-confined CoP-CoO nanoheterostructure with strong interfacial synergy triggered the robust hydrogen evolution from ammonia borane. *J. Energy Chem.* **2021**, *57*, 198–205.

[4] Xiao, X.; Yang, L. J.; Sun, W. P.; Chen, Y.; Yu, H.; Li, K. K.; Jia, B. H.; Zhang, L.; Ma, T. Y. Electrocatalytic water splitting: From harsh and mild conditions to natural seawater. *Small* **2022**, *18*, 2105830.

[5] Song, J. J.; Wei, C.; Huang, Z. F.; Liu, C. T.; Zeng, L.; Wang, X.; Xu, Z. J. A review on fundamentals for designing oxygen evolution electrocatalysts. *Chem. Soc. Rev.* **2020**, *49*, 2196–2214.

[6] Gao, F.; He, J. Q.; Wang, H. W.; Lin, J. H.; Chen, R. X.; Yi, K.; Huang, F.; Lin, Z.; Wang, M. Y. Te-mediated electro-driven oxygen evolution reaction. *Nano Res. Energy* **2022**, *1*, e9120029.

[7] Wei, Z. H.; Liu, Y.; Peng, Z. K.; Song, H. Q.; Liu, Z. Y.; Liu, B. Z.; Li, B. J.; Yang, B.; Lu, S. Y. Cobalt-ruthenium nanoalloys parceled in porous nitrogen-doped graphene as highly efficient difunctional catalysts for hydrogen evolution reaction and hydrolysis of ammonia borane. *ACS Sustainable Chem. Eng.* **2019**, *7*, 7014–7023.

[8] Wang, L. P.; Wu, X. Q.; Guo, S. J.; Han, M. M.; Zhou, Y. J.; Sun, Y.; Huang, H.; Liu, Y.; Kang, Z. H. Mesoporous nitrogen, sulfur co-doped carbon dots/CoS hybrid as an efficient electrocatalyst for hydrogen evolution. *J. Mater. Chem. A* **2017**, *5*, 2717–2723.

[9] Liu, Y.; Yong, X.; Liu, Z. Y.; Chen, Z. M.; Kang, Z. H.; Lu, S. Y. Unified catalyst for efficient and stable hydrogen production by both the electrolysis of water and the hydrolysis of ammonia borane. *Adv. Sustain. Syst.* **2019**, *3*, 1800161.

[10] Zheng, X. B.; Yang, J. R.; Xu, Z. F.; Wang, Q. S.; Wu, J. B.; Zhang, E. H.; Dou, S. X.; Sun, W. P.; Wang, D. S.; Li, Y. D. Ru-Co pair sites catalyst boosts the energetics for the oxygen evolution reaction. *Angew. Chem., Int. Ed.* **2022**, *61*, e202205946.

[11] Jing, H. Y.; Zhu, P.; Zheng, X. B.; Zhang, Z. D.; Wang, D. S.; Li, Y. D. Theory-oriented screening and discovery of advanced energy transformation materials in electrocatalysis. *Adv. Powder Mater.* **2022**, *1*, 100013.

[12] Song, H. Q.; Wu, M.; Tang, Z. Y.; Tse, J. S.; Yang, B.; Lu, S. Y. Single atom ruthenium-doped CoP/CDs nanosheets via splicing of carbon-dots for robust hydrogen production. *Angew. Chem., Int. Ed.* **2021**, *60*, 7234–7244.

[13] Wang, Q.; Zhang, Z.; Cai, C.; Wang, M. Y.; Zhao, Z. L.; Li, M. H.; Huang, X.; Han, S. B.; Zhou, H.; Feng, Z. X. et al. Single iridium atom doped Ni_2P catalyst for optimal oxygen evolution. *J. Am. Chem. Soc.* **2021**, *143*, 13605–13615.

[14] Wu, H.; Lu, S. Y.; Yang, B. Carbon-dot-enhanced electrocatalytic hydrogen evolution. *Acc. Mater. Res.* **2022**, *3*, 319–330.

[15] Song, H. Q.; Yu, J. K.; Tang, Z. Y.; Yang, B.; Lu, S. Y. Halogen-doped carbon dots on amorphous cobalt phosphide as robust electrocatalysts for overall water splitting. *Adv. Energy Mater.* **2022**, *12*, 2102573.

[16] Li, W. H.; Yang, J. R.; Wang, D. S. Long-range interactions in diatomic catalysts boosting electrocatalysis. *Angew. Chem., Int. Ed.* **2022**, *61*, e202213318.

[17] Zhao, F.; Wen, B.; Niu, W. H.; Chen, Z.; Yan, C.; Selloni, A.; Tully, C. G.; Yang, X. F.; Koel, B. E. Increasing iridium oxide

activity for the oxygen evolution reaction with hafnium modification. *J. Am. Chem. Soc.* **2021**, *143*, 15616–15623.

[18] Wang, C.; Zhai, P. L.; Xia, M. Y.; Wu, Y. Z.; Zhang, B.; Li, Z. W.; Ran, L.; Gao, J. F.; Zhang, X. M.; Fan, Z. Z. et al. Engineering lattice oxygen activation of iridium clusters stabilized on amorphous bimetal borides array for oxygen evolution reaction. *Angew. Chem., Int. Ed.* **2021**, *60*, 27126–27134.

[19] Ma, P. Y.; Feng, C.; Kong, Y.; Wang, D. D.; Zuo, M.; Wang, S. C.; Wang, R. Y.; Kuang, L. L.; Ding, X. L.; Zhou, S. M. et al. Modulating hydrogen bonding in single-atom catalysts to break scaling relation for oxygen evolution. *Chem Catal.* **2022**, *2*, 2764–2777.

[20] Zhao, S. Y.; Berry-Gair, J.; Li, W. Y.; Guan, G. Q.; Yang, M. N.; Li, J. W.; Lai, F. L.; Corà, F.; Holt, K.; Brett, D. J. L. et al. The role of phosphate group in doped cobalt molybdate: Improved electrocatalytic hydrogen evolution performance. *Adv. Sci.* **2020**, *7*, 1903674.

[21] Zaik, K.; Werle, S. Solar and wind energy in Poland as power sources for electrolysis process—A review of studies and experimental methodology. *Int. J. Hydrogen Energy*, in press,https://doi.org.10.1016/j.ijhydene.2022.02.074.

[22] AlRafea, K.; Fowler, M.; Elkamel, A.; Hajimiragha, A. Integration of renewable energy sources into combined cycle power plants through electrolysis generated hydrogen in a new designed energy hub. *Int. J. Hydrogen Energy* **2016**, *41*, 16718–16728.

[23] Yu, P.; Wang, F. M.; Shifa, T. A.; Zhan, X. Y.; Lou, X. D.; Xia, F.; He, J. Earth abundant materials beyond transition metal dichalcogenides: A focus on electrocatalyzing hydrogen evolution reaction. *Nano Energy* **2019**, *58*, 244–276.

[24] Cheng, Y. F.; Fan, X.; Liao, F.; Lu, S. K.; Li, Y. Y.; Liu, L. B.; Li, Y. Q.; Lin, H. P.; Shao, M. W.; Lee, S. T. Os/Si nanocomposites as excellent hydrogen evolution electrocatalysts with thermodynamically more favorable hydrogen adsorption free energy than platinum. *Nano Energy* **2017**, *39*, 284–290.

[25] Montoya, J. H.; Seitz, L. C.; Chakthranont, P.; Vojvodic, A.; Jaramillo, T. F.; Nørskov, J. K. Materials for solar fuels and chemicals. *Nat. Mater.* **2017**, *16*, 70–81.

[26] Zhang, B.; Zheng, X. L.; Voznyy, O.; Comin, R.; Bajdich, M.; García-Melchor, M.; Han, L. L.; Xu, J. X.; Liu, M.; Zheng, L. R. et al. Homogeneously dispersed multimetal oxygen-evolving catalysts. *Science* **2016**, *352*, 333–337.

[27] Huang, Z. F.; Xi, S. B.; Song, J. J.; Dou, S.; Li, X. G.; Du, Y. H.; Diao, C. Z.; Xu, Z. J.; Wang, X. Tuning of lattice oxygen reactivity and scaling relation to construct better oxygen evolution electrocatalyst. *Nat. Commun.* **2021**, *12*, 3992.

[28] Zhao, G. Q.; Li, P.; Cheng, N. Y.; Dou, S. X.; Sun, W. P. An $Ir/Ni(OH)_2$ heterostructured electrocatalyst for the oxygen evolution reaction: Breaking the scaling relation, stabilizing iridium(V), and beyond. *Adv. Mater.* **2020**, *32*, 2000872.

[29] Wen, Y. Z.; Chen, P. N.; Wang, L.; Li, S. Y.; Wang, Z. Y.; Abed, J.; Mao, X. N.; Min, Y. M.; Dinh, C. T.; De Luna, P. et al. Stabilizing highly active Ru sites by suppressing lattice oxygen participation in acidic water oxidation. *J. Am. Chem. Soc.* **2021**, *143*, 6482–6490.

[30] Jin, H.; Choi, S.; Bang, G. J.; Kwon, T.; Kim, H. S.; Lee, S. J.; Hong, Y.; Lee, D. W.; Park, H. S.; Baik, H. et al. Safeguarding the RuO_2 phase against lattice oxygen oxidation during acidic water electrooxidation. *Energy Environ. Sci.* **2022**, *15*, 1119–1130.

[31] Song, F.; Busch, M. M.; Lassalle-Kaiser, B.; Hsu, C. S.; Petkucheva, E.; Bensimon, M.; Chen, H. M.; Corminboeuf, C.; Hu, X. L. An unconventional iron nickel catalyst for the oxygen evolution reaction. *ACS Cent. Sci.* **2019**, *5*, 558–568.

[32] Lin, C.; Li, J. L.; Li, X. P.; Yang, S.; Luo, W.; Zhang, Y. J.; Kim, S. H.; Kim, D. H.; Shinde, S. S.; Li, Y. F. et al. *In-situ* reconstructed Ru atom array on α-MnO_2 with enhanced performance for acidic water oxidation. *Nat. Catal.* **2021**, *4*, 1012–1023.

[33] Huang, Z. F.; Song, J. J.; Du, Y. H.; Xi, S. B.; Dou, S.; Nsanzimana, J. M. V.; Wang, C.; Xu, Z. J.; Wang, X. Chemical and structural origin of lattice oxygen oxidation in Co-Zn oxyhydroxide oxygen evolution electrocatalysts. *Nat. Energy* **2019**, *4*, 329–338.

[34] Chen, X.; Wang, Q. C.; Cheng, Y. W.; Xing, H. L.; Li, J. Z.; Zhu, X. J.; Ma, L. B.; Li, Y. T.; Liu, D. M. S-doping triggers redox reactivities of both iron and lattice oxygen in FeOOH for low-cost and high-performance water oxidation. *Adv. Funct. Mater.* **2022**, *32*, 2112674.

[35] Zhang, X. H.; Chen, Q. F.; Deng, J. T.; Xu, X. Y.; Zhan, J. R.; Du, H. Y.; Yu, Z. Y.; Li, M. X.; Zhang, M. T.; Shao, Y. H. Identifying metal-oxo/peroxo intermediates in catalytic water oxidation by *in situ* electrochemical mass spectrometry. *J. Am. Chem. Soc.* **2022**, *144*, 17748–17752.

[36] Feng, C.; Zhang, Z. R.; Wang, D. D.; Kong, Y.; Wei, J.; Wang, R. Y.; Ma, P. Y.; Li, H. L.; Geng, Z. G.; Zuo, M. et al. Tuning the electronic and steric interaction at the atomic interface for enhanced oxygen evolution. *J. Am. Chem. Soc.* **2022**, *144*, 9271–9279.

[37] Yang, X. G.; Wang, Y. X.; Li, C. M.; Wang, D. W. Mechanisms of water oxidation on heterogeneous catalyst surfaces. *Nano Res.* **2021**, *14*, 3446–3457.

[38] Zhang, Y. K.; Wu, C. Q.; Jiang, H. L.; Lin, Y. X.; Liu, H. J.; He, Q.; Chen, S. M.; Duan, T.; Song, L. Atomic iridium incorporated in cobalt hydroxide for efficient oxygen evolution catalysis in neutral electrolyte. *Adv. Mater.* **2018**, *30*, 1707522.

[39] Li, W. D.; Wei, Z. H.; Wang, B. Y.; Liu, Y.; Song, H. Q.; Tang, Z. Y.; Yang, B.; Lu, S. Y. Carbon quantum dots enhanced the activity for the hydrogen evolution reaction in ruthenium-based electrocatalysts. *Mater. Chem. Front.* **2020**, *4*, 277–284.

[40] Wang, J.; Yang, H.; Li, F.; Li, L. G.; Wu, J. B.; Liu, S. H.; Cheng, T.; Xu, Y.; Shao, Q.; Huang, X. Q. Single-site Pt-doped RuO_2 hollow nanospheres with interstitial C for high-performance acidic overall water splitting. *Sci. Adv.* **2022**, *8*, eabl9271.

[41] Li, C. Q.; Baek, J. B. Recent advances in noble metal (Pt, Ru, and Ir)-based electrocatalysts for efficient hydrogen evolution reaction. *ACS Omega* **2020**, *5*, 31–40.

[42] Xu, W. J.; Chang, J. F.; Cheng, Y. G.; Liu, H. Q.; Li, J. F.; Ai, Y. J.; Hu, Z. N.; Zhang, X. Y.; Wang, Y. M.; Liang, Q. L. et al. A multi-step induced strategy to fabricate core–shell Pt-Ni alloy as symmetric electrocatalysts for overall water splitting. *Nano Res.* **2022**, *15*, 965–971.

[43] Zhang, S.; Zhang, X.; Shi, X. R.; Zhou, F.; Wang, R. H.; Li, X. J. Facile fabrication of ultrafine nickel-iridium alloy nanoparticles/graphene hybrid with enhanced mass activity and stability for overall water splitting. *J. Energy Chem.* **2020**, *49*, 166–173.

[44] Bao, M. J.; Amiinu, I. S.; Peng, T.; Li, W. Q.; Liu, S. J.; Wang, Z.; Pu, Z. H.; He, D. P.; Xiong, Y. L.; Mu, S. C. Surface evolution of PtCu alloy shell over Pd nanocrystals leads to superior hydrogen evolution and oxygen reduction reactions. *ACS Energy Lett.* **2018**, *3*, 940–945.

[45] Pang, B. B.; Liu, X. K.; Liu, T. Y.; Chen, T.; Shen, X. Y.; Zhang, W.; Wang, S. C.; Liu, T.; Liu, D.; Ding, T. et al. Laser-assisted high-performance PtRu alloy for pH-universal hydrogen evolution. *Energy Environ. Sci.* **2022**, *15*, 102–108.

[46] Li, W. D.; Liu, Y.; Wang, B. Y.; Song, H. Q.; Liu, Z. Y.; Lu, S. Y.; Yang, B. Kilogram-scale synthesis of carbon quantum dots for hydrogen evolution, sensing and bioimaging. *Chin. Chem. Lett.* **2019**, *30*, 2323–2327.

[47] Shen, F.; Wang, Y. M.; Qian, G. F.; Chen, W.; Jiang, W. J.; Luo, L.; Yin, S. B. Bimetallic iron-iridium alloy nanoparticles supported on nickel foam as highly efficient and stable catalyst for overall water splitting at large current density. *Appl. Catal. B:Environ.* **2020**, *278*, 119327.

[48] Wu, Q. L.; Luo, M.; Han, J. H.; Peng, W.; Zhao, Y.; Chen, D. C.; Peng, M.; Liu, J.; De Groot, F. M. F.; Tan, Y. W. Identifying electrocatalytic sites of the nanoporous copper-ruthenium alloy for hydrogen evolution reaction in alkaline electrolyte. *ACS Energy Lett.* **2020**, *5*, 192–199.

[49] Sun, X. C.; Liu, F.; Chen, X.; Li, C. C.; Yu, J.; Pan, M. Iridium-doped ZIFs-derived porous carbon-coated IrCo alloy as competent bifunctional catalyst for overall water splitting in acid medium. *Electrochim. Acta* **2019**, *307*, 206–213.

[50] Vassalini, I.; Borgese, L.; Mariz, M.; Polizzi, S.; Aquilanti, G.;

Ghigna, P.; Sartorel, A.; Amendola, V.; Alessandri, I. Enhanced electrocatalytic oxygen evolution in Au-Fe nanoalloys. *Angew. Chem., Int. Ed.* **2017**, *56*, 6589–6593.

[51] Liu, Y.; Li, X.; Zhang, Q. H.; Li, W. D.; Xie, Y.; Liu, H. Y.; Shang, L.; Liu, Z. Y.; Chen, Z. M.; Gu, L. et al. A general route to prepare low-ruthenium-content bimetallic electrocatalysts for pH-universal hydrogen evolution reaction by using carbon quantum dots. *Angew. Chem., Int. Ed.* **2020**, *59*, 1718–1726.

[52] Katiyar, N. K.; Biswas, K.; Yeh, J. W.; Sharma, S.; Tiwary, C. S. A perspective on the catalysis using the high entropy alloys. *Nano Energy* **2021**, *88*, 106261.

[53] Sharma, L.; Katiyar, N. K.; Parui, A.; Das, R.; Kumar, R.; Tiwary, C. S.; Singh, A. K.; Halder, A.; Biswas, K. Low-cost high entropy alloy (HEA) for high-efficiency oxygen evolution reaction (OER). *Nano Res.* **2022**, *15*, 4799–4806.

[54] Chang, S. Q.; Cheng, C. C.; Cheng, P. Y.; Huang, C. L.; Lu, S. Y. Pulse electrodeposited FeCoNiMnW high entropy alloys as efficient and stable bifunctional electrocatalysts for acidic water splitting. *Chem. Eng. J.* **2022**, *446*, 137452.

[55] Wang, S. Q.; Xu, B. L.; Huo, W. Y.; Feng, H. C.; Zhou, X. F.; Fang, F.; Xie, Z. H.; Shang, J. K.; Jiang, J. Q. Efficient FeCoNiCuPd thin-film electrocatalyst for alkaline oxygen and hydrogen evolution reactions. *Appl. Catal. B:Environ.* **2022**, *313*, 121472.

[56] Gao, Y. X.; Zheng, D. B.; Li, Q. C.; Xiao, W. P.; Ma, T. Y.; Fu, Y. L.; Wu, Z. X.; Wang, L. 3D Co_3O_4-RuO_2 hollow spheres with abundant interfaces as advanced trifunctional electrocatalyst for water-splitting and flexible Zn-air battery. *Adv. Funct. Mater.* **2022**, *32*, 2203206.

[57] Chang, J. W.; Song, X. D.; Yu, C.; Yu, J. H.; Ding, Y. W.; Yao, C.; Zhao, Z. B.; Qiu, J. S. Hydrogen-bonding triggered assembly to configure hollow carbon nanosheets for highly efficient tri-iodide reduction. *Adv. Funct. Mater.* **2020**, *30*, 2006270.

[58] Pan, J.; Yu, S. W.; Jing, Z. W.; Zhou, Q. T.; Dong, Y. F.; Lou, X. D.; Xia, F. Electrocatalytic hydrogen evolution reaction related to nanochannel materials. *Small Struct.* **2021**, *2*, 2100076.

[59] Zhang, Q.; Xiao, W.; Guo, W. H.; Yang, Y. X.; Lei, J. L.; Luo, H. Q.; Li, N. B. Macroporous array induced multiscale modulation at the surface/interface of $Co(OH)_2$/NiMo self-supporting electrode for effective overall water splitting. *Adv. Funct. Mater.* **2021**, *31*, 2102117.

[60] Huan, Y. H.; Shi, J. P.; Zou, X. L.; Gong, Y.; Xie, C. Y.; Yang, Z. J.; Zhang, Z. P.; Gao, Y.; Shi, Y. P.; Li, M. H. et al. Scalable production of two-dimensional metallic transition metal dichalcogenide nanosheet powders using NaCl templates toward electrocatalytic applications. *J. Am. Chem. Soc.* **2019**, *141*, 18694–18703.

[61] Liu, Z. H.; Du, Y.; Yu, R. H.; Zheng, M. B.; Hu, R.; Wu, J. S.; Xia, Y. Y.; Zhuang, Z. C.; Wang, D. S. Tuning mass transport in electrocatalysis down to sub-5 nm through nanoscale grade separation. *Angew. Chem., Int. Ed.* **2023**, *62*, e202212653.

[62] Zhu, Y. P.; Ma, T. Y.; Jaroniec, M.; Qiao, S. Z. Self-templating synthesis of hollow Co_3O_4 microtube arrays for highly efficient water electrolysis. *Angew. Chem., Int. Ed.* **2017**, *56*, 1324–1328.

[63] Zhou, J. Q.; Yu, L.; Zhou, Q. C.; Huang, C. Q.; Zhang, Y. L.; Yu, B.; Yu, Y. Ultrafast fabrication of porous transition metal foams for efficient electrocatalytic water splitting. *Appl. Catal. B:Environ.* **2021**, *288*, 120002.

[64] Li, R. Q.; Wang, B. L.; Gao, T.; Zhang, R.; Xu, C. Y.; Jiang, X. F.; Zeng, J. J.; Bando, Y.; Hu, P. F.; Li, Y. L. et al. Monolithic electrode integrated of ultrathin NiFeP on 3D strutted graphene for bifunctionally efficient overall water splitting. *Nano Energy* **2019**, *58*, 870–876.

[65] Zhang, X.; Zhang, X.; Xu, H. M.; Wu, Z. S.; Wang, H. L.; Liang, Y. Y. Iron-doped cobalt monophosphide nanosheet/carbon nanotube hybrids as active and stable electrocatalysts for water splitting. *Adv. Funct. Mater.* **2017**, *27*, 1606635.

[66] Li, W. D.; Liu, Y.; Wu, M.; Feng, X. L.; Redfern, S. A. T.; Shang, Y.; Yong, X.; Feng, T. L.; Wu, K. F.; Liu, Z. Y. et al. Carbon-quantum-dots-loaded ruthenium nanoparticles as an efficient electrocatalyst for hydrogen production in alkaline media. *Adv. Mater.* **2018**, *30*, 1800676.

[67] Wang, X. Y.; Fei, Y.; Chen, J.; Pan, Y. X.; Yuan, W. Y.; Zhang, L. Y.; Guo, C. X.; Li, C. M. Directionally *in situ* self-assembled, high-density, macropore-oriented, CoP-impregnated, 3D hierarchical porous carbon sheet nanostructure for superior electrocatalysis in the hydrogen evolution reaction. *Small* **2022**, *18*, 2103866.

[68] Shi, Z. P.; Li, J.; Jiang, J. D.; Wang, Y. B.; Wang, X.; Li, Y.; Yang, L. T.; Chu, Y. Y.; Bai, J. S.; Yang, J. H. et al. Enhanced acidic water oxidation by dynamic migration of oxygen species at the Ir/Nb_2O_{5-x} catalyst/support interfaces. *Angew. Chem., Int. Ed.* **2022**, *61*, e202212341.

[69] Wu, H.; Wu, M.; Wang, B. Y.; Yong, X.; Liu, Y. S.; Li, B. J.; Liu, B. Z.; Lu, S. Y. Interface electron collaborative migration of Co-Co_3O_4/carbon dots: Boosting the hydrolytic dehydrogenation of ammonia borane. *J. Energy Chem.* **2020**, *48*, 43–53.

[70] Jiang, Z. L.; Song, S. J.; Zheng, X. B.; Liang, X.; Li, Z. X.; Gu, H. F.; Li, Z.; Wang, Y.; Liu, S. H.; Chen, W. X. et al. Lattice strain and Schottky junction dual regulation boosts ultrafine ruthenium nanoparticles anchored on a N-modified carbon catalyst for H_2 production. *J. Am. Chem. Soc.* **2022**, *144*, 19619–19626.

[71] Xue, Z. H.; Su, H.; Yu, Q. Y.; Zhang, B.; Wang, H. H.; Li, X. H.; Chen, J. S. Janus Co/CoP nanoparticles as efficient Mott−Schottky electrocatalysts for overall water splitting in wide pH range. *Adv. Energy Mater.* **2017**, *7*, 1602355.

[72] Yang, J. R.; Li, W. H.; Tan, S. D.; Xu, K. N.; Wang, Y.; Wang, D. S.; Li, Y. D. The electronic metal−support interaction directing the design of single atomic site catalysts: Achieving high efficiency towards hydrogen evolution. *Angew. Chem., Int. Ed.* **2021**, *60*, 19085–19091.

[73] Zhang, Y. Y.; Huang, H.; Han, Y.; Qin, Y. N.; Nie, N. Z.; Cai, W. W.; Zhang, X. Y.; Li, Z. J.; Lai, J. P.; Wang, L. Constructing stable charge redistribution through strong metal−support interaction for overall water splitting in acidic solution. *J. Mater. Chem. A* **2022**, *10*, 13241–13246.

[74] Zhan, G.; Zhang, J. F.; Wang, Y.; Yu, C. P.; Wu, J. J.; Cui, J. W.; Shu, X.; Qin, Y. Q.; Zheng, H. M.; Sun, J. et al. MoS_2 quantum dots decorated ultrathin NiO nanosheets for overall water splitting. *J. Colloid Interface Sci.* **2020**, *566*, 411–418.

[75] Liu, J.; Wang, Z. C.; Wu, X. K.; Zhang, D.; Zhang, Y.; Xiong, J.; Wu, Z. X.; Lai, J. P.; Wang, L. Pt doping and strong metal−support interaction as a strategy for NiMo-based electrocatalysts to boost the hydrogen evolution reaction in alkaline solution. *J. Mater. Chem. A* **2022**, *10*, 15395–15401.

[76] Liu, Y. K.; Jiang, S.; Li, S. J.; Zhou, L.; Li, Z. H.; Li, J. M.; Shao, M. F. Interface engineering of (Ni, Fe)S_2@MoS_2 heterostructures for synergetic electrochemical water splitting. *Appl. Catal. B:Environ.* **2019**, *247*, 107–114.

[77] Wang, L. G.; Duan, X. X.; Liu, X. J.; Gu, J.; Si, R.; Qiu, Y.; Qiu, Y. M.; Shi, D. E.; Chen, F. H.; Sun, X. M. et al. Atomically dispersed Mo supported on metallic Co_9S_8 nanoflakes as an advanced noble-metal-free bifunctional water splitting catalyst working in universal pH conditions. *Adv. Energy Mater.* **2020**, *10*, 1903137.

[78] Ge, Y. Y.; Wang, X. X.; Chen, B.; Huang, Z. Q.; Shi, Z. Y.; Huang, B.; Liu, J. W.; Wang, G.; Chen, Y.; Li, L. J. et al. Preparation of fcc-2H-fcc heterophase Pd@Ir nanostructures for high-performance electrochemical hydrogen evolution. *Adv. Mater.* **2022**, *34*, 2107399.

[79] Hu, F.; Yu, D. S.; Ye, M.; Wang, H.; Hao, Y. N.; Wang, L. Q.; Li, L. L.; Han, X. P.; Peng, S. J. Lattice-matching formed mesoporous transition metal oxide heterostructures advance water splitting by active Fe-O-Cu bridges. *Adv. Energy Mater.* **2022**, *12*, 2200067.

[80] Wang, L. G.; Liu, H.; Zhuang, J. H.; Wang, D. S. Small-scale big science: From nano- to atomically dispersed catalytic materials. *Small Sci.* **2022**, *2*, 2200036.

[81] Wang, L. G.; Wang, D. S.; Li, Y. D. Single-atom catalysis for carbon neutrality. *Carbon Energy* **2022**, *4*, 1021–1079.

[82] Cheng, Y. J.; Song, H. Q.; Yu, J. K.; Chang, J. W.; Waterhouse, G. I. N.; Tang, Z. Y.; Yang, B.; Lu, S. Y. Carbon dots-derived carbon nanoflowers decorated with cobalt single atoms and nanoparticles as efficient electrocatalysts for oxygen reduction. *Chin. J. Catal.*

2022, *43*, 2443–2452.
[83] Yu, J.; Li, J.; Xu, C. Y.; Li, Q. Q.; Liu, Q.; Liu, J. Y.; Chen, R. R.; Zhu, J. H.; Wang, J. Modulating the d-band centers by coordination environment regulation of single-atom Ni on porous carbon fibers for overall water splitting. *Nano Energy* **2022**, *98*, 107266.
[84] Shi, G. Y.; Tano, T.; Tryk, D. A.; Yamaguchi, M.; Iiyama, A.; Uchida, M.; Iida, K.; Arata, C.; Watanabe, S.; Kakinuma, K. Temperature dependence of oxygen evolution reaction activity in alkaline solution at Ni-Co oxide catalysts with amorphous/crystalline surfaces. *ACS Catal.* **2022**, *12*, 14209–14219.
[85] Liu, S. D.; Li, H. K.; Zhong, J.; Xu, K.; Wu, G.; Liu, C.; Zhou, B. B.; Yan, Y.; Li, L. X.; Cha, W. H. et al. A crystal glass-nanostructured Al-based electrocatalyst for hydrogen evolution reaction. *Sci. Adv.* **2022**, *8*, eadd6421.
[86] Gong, Z. C.; Liu, R.; Gong, H. S.; Ye, G. L.; Liu, J. J.; Dong, J. C.; Liao, J. W.; Yan, M. M.; Liu, J. B.; Huang, K. et al. Constructing a graphene-encapsulated amorphous/crystalline heterophase NiFe alloy by microwave thermal shock for boosting the oxygen evolution reaction. *ACS Catal.* **2021**, *11*, 12284–12292.
[87] Cheng, Y. J.; Song, H. Q.; Wu, H.; Zhang, P. K.; Tang, Z. Y.; Lu, S. Y. Defects enhance the electrocatalytic hydrogen evolution properties of MoS_2-based materials. *Chem. Asian J.* **2020**, *15*, 3123–3134.
[88] Chang, J. W.; Song, X. D.; Yu, C.; Huang, H. W.; Hong, J. F.; Ding, Y. W.; Huang, H. L.; Yu, J. H.; Tan, X. Y.; Zhao, Z. B. et al. Gravity field-mediated synthesis of carbon-conjugated quantum dots with tunable defective density for enhanced triiodide reduction. *Nano Energy* **2020**, *69*, 104377.
[89] Fang, F.; Wang, Y.; Shen, L. W.; Tian, G.; Cahen, D.; Xiao, Y. X.; Chen, J. B.; Wu, S. M.; He, L.; Ozoemena, K. I. et al. Interfacial carbon makes nano-particulate RuO_2 an efficient, stable, pH-universal catalyst for splitting of seawater. *Small* **2022**, *18*, 2203778.
[90] Shah, K.; Dai, R. Y.; Mateen, M.; Hassan, Z.; Zhuang, Z. W.; Liu, C. H.; Israr, M.; Cheong, W. C.; Hu, B. T.; Tu, R. Y. et al. Cobalt single atom incorporated in ruthenium oxide sphere: A robust bifunctional electrocatalyst for HER and OER. *Angew. Chem., Int. Ed.* **2022**, *61*, e202114951.
[91] Yan, P. X.; Huang, M. L.; Wang, B. Z.; Wan, Z. X.; Qian, M. C.; Yan, H.; Isimjan, T. T.; Tian, J. N.; Yang, X. L. Oxygen defect-rich double-layer hierarchical porous Co_3O_4 arrays as high-efficient oxygen evolution catalyst for overall water splitting. *J. Energy Chem.* **2020**, *47*, 299–306.
[92] Cao, X.; Panizon, E.; Vanossi, A.; Manini, N.; Tosatti, E.; Bechinger, C. Pile-up transmission and reflection of topological defects at grain boundaries in colloidal crystals. *Nat. Commun.* **2020**, *11*, 3079.
[93] Zhu, J. T.; Tu, Y. D.; Cai, L. J.; Ma, H. B.; Chai, Y.; Zhang, L. F.; Zhang, W. J. Defect-assisted anchoring of Pt single atoms on MoS_2 nanosheets produces high-performance catalyst for industrial hydrogen evolution reaction. *Small* **2022**, *18*, 2104824.
[94] Chen, Y. W.; Ding, R.; Li, J.; Liu, J. G. Highly active atomically dispersed platinum-based electrocatalyst for hydrogen evolution reaction achieved by defect anchoring strategy. *Appl. Catal. B:Environ.* **2022**, *301*, 120830.
[95] Xie, J. F.; Gao, L.; Jiang, H. L.; Zhang, X. D.; Lei, F. C.; Hao, P.; Tang, B.; Xie, Y. Platinum nanocrystals decorated on defect-rich MoS_2 nanosheets for pH-universal hydrogen evolution reaction. *Cryst. Growth Des.* **2019**, *19*, 60–65.
[96] Zhang, J. Q.; Zhao, Y. F.; Guo, X.; Chen, C.; Dong, C. L.; Liu, R. S.; Han, C. P.; Li, Y. D.; Gogotsi, Y.; Wang, G. X. Single platinum atoms immobilized on an MXene as an efficient catalyst for the hydrogen evolution reaction. *Nat. Catal.* **2018**, *1*, 985–992.
[97] Zong, R. Q.; Fang, Y. G.; Zhu, C. R.; Zhang, X.; Wu, L.; Hou, X.; Tao, Y. K.; Shao, J. Surface defect engineering on perovskite oxides as efficient bifunctional electrocatalysts for water splitting. *ACS Appl. Mater. Interfaces* **2021**, *13*, 42852–42860.
[98] Su, H.; Jiang, J.; Li, N.; Gao, Y. Q.; Ge, L. NiCu alloys anchored defect-rich NiFe layered double-hydroxides as efficient electrocatalysts for overall water splitting. *Chem. Eng. J.* **2022**, *446*, 137226.
[99] Ren, K.; Yin, P. F.; Zhou, Y. Z.; Cao, X. Z.; Dong, C. K.; Cui, L.; Liu, H.; Du, X. W. Localized defects on copper sulfide surface for enhanced plasmon resonance and water splitting. *Small* **2017**, *13*, 1700867.
[100] Yamazaki, Y.; Mori, K.; Kuwahara, Y.; Kobayashi, H.; Yamashita, H. Defect engineering of Pt/TiO_{2-x} photocatalysts via reduction treatment assisted by hydrogen spillover. *ACS Appl. Mater. Interfaces* **2021**, *13*, 48669–48678.
[101] Chen, K.; Huan, Y. H.; Quan, W. Z.; Zhu, L. J.; Fu, J. T.; Hu, J. Y.; Cui, F. F.; Zhou, F.; Wang, X. Z.; Li, M. J. et al. Controllable growth and defect engineering of vertical $PtSe_2$ nanosheets for electrocatalytic hydrogen evolution. *ACS Energy Lett.* **2022**, *7*, 3675–3684.
[102] Peng, S. J.; Gong, F.; Li, L. L.; Yu, D. S.; Ji, D. X.; Zhang, T. R.; Hu, Z.; Zhang, Z. Q.; Chou, S. L.; Du, Y. H. et al. Necklace-like multishelled hollow spinel oxides with oxygen vacancies for efficient water electrolysis. *J. Am. Chem. Soc.* **2018**, *140*, 13644–13653.
[103] Xu, L.; Jiang, Q. Q.; Xiao, Z. H.; Li, X. Y.; Huo, J.; Wang, S. Y.; Dai, L. M. Plasma-engraved Co_3O_4 nanosheets with oxygen vacancies and high surface area for the oxygen evolution reaction. *Angew. Chem., Int. Ed.* **2016**, *55*, 5277–5281.
[104] Liu, S. L.; Shen, Y.; Zhang, Y.; Cui, B. H.; Xi, S. B.; Zhang, J. F.; Xu, L. Y.; Zhu, S. Z.; Chen, Y. N.; Deng, Y. D. et al. Extreme environmental thermal shock induced dislocation-rich Pt nanoparticles boosting hydrogen evolution reaction. *Adv. Mater.* **2022**, *34*, 2106973.
[105] Chang, J. W.; Yu, C.; Song, X. D.; Han, X. T.; Ding, Y. W.; Tan, X. Y.; Li, S. F.; Xie, Y. Y.; Zhao, Z. B.; Qiu, J. S. Mechanochemistry-driven prelinking enables ultrahigh nitrogen-doping in carbon materials for triiodide reduction. *Nano Energy* **2021**, *89*, 106332.
[106] Ding, P.; Song, H. Q.; Chang, J. W.; Lu, S. Y. N-doped carbon dots coupled NiFe-LDH hybrids for robust electrocatalytic alkaline water and seawater oxidation. *Nano Res.* **2022**, *15*, 7063–7070.
[107] Chang, J. W.; Yu, C.; Song, X. D.; Tan, X. Y.; Ding, Y. W.; Zhao, Z. B.; Qiu, J. S. A C-S-C linkage-triggered ultrahigh nitrogen-doped carbon and the identification of active site in triiodide reduction. *Angew. Chem., Int. Ed.* **2021**, *60*, 3587–3595.
[108] Wang, J.; Cheng, C.; Yuan, Q.; Yang, H.; Meng, F. Q.; Zhang, Q. H.; Gu, L.; Cao, J. L.; Li, L. G.; Haw, S. C. et al. Exceptionally active and stable RuO_2 with interstitial carbon for water oxidation in acid. *Chem* **2022**, *8*, 1673–1687.
[109] Song, H. Q.; Li, Y. H.; Shang, L.; Tang, Z. Y.; Zhang, T. R.; Lu, S. Y. Designed controllable nitrogen-doped carbon-dots-loaded MoP nanoparticles for boosting hydrogen evolution reaction in alkaline medium. *Nano Energy* **2020**, *72*, 104730.
[110] Yao, Y. C.; Hu, S. L.; Chen, W. X.; Huang, Z. Q.; Wei, W. C.; Yao, T.; Liu, R. R.; Zang, K. T.; Wang, X. Q.; Wu, G. et al. Engineering the electronic structure of single atom Ru sites via compressive strain boosts acidic water oxidation electrocatalysis. *Nat. Catal.* **2019**, *2*, 304–313.
[111] Qin, Y.; Yu, T. T.; Deng, S. H.; Zhou, X. Y.; Lin, D. M.; Zhang, Q.; Jin, Z. Y.; Zhang, D. F.; He, Y. B.; Qiu, H. J. et al. RuO_2 electronic structure and lattice strain dual engineering for enhanced acidic oxygen evolution reaction performance. *Nat. Commun.* **2022**, *13*, 3784.
[112] Wang, Y.; Li, X. P.; Zhang, M. M.; Zhou, Y. G.; Rao, D. W.; Zhong, C.; Zhang, J. F.; Han, X. P.; Hu, W. B.; Zhang, Y. C. et al. Lattice-strain engineering of homogeneous $NiS_{0.5}Se_{0.5}$ core–shell nanostructure as a highly efficient and robust electrocatalyst for overall water splitting. *Adv. Mater.* **2020**, *32*, 2000231.
[113] Sun, L.; Dai, Z. F.; Zhong, L. X.; Zhao, Y. W.; Cheng, Y.; Chong, S. K.; Chen, G. J.; Yan, C. S.; Zhang, X. Y.; Tan, H. T. et al. Lattice strain and atomic replacement of CoO_6 octahedra in layered sodium cobalt oxide for boosted water oxidation electrocatalysis. *Appl. Catal. B:Environ.* **2021**, *297*, 120477.
[114] Wu, G.; Han, X.; Cai, J. Y.; Yin, P. Q.; Cui, P. X.; Zheng, X. S.; Li, H.; Chen, C.; Wang, G. M.; Hong, X. In-plane strain engineering in ultrathin noble metal nanosheets boosts the intrinsic electrocatalytic

hydrogen evolution activity. *Nat. Commun.* **2022**, *13*, 4200.
[115] Li, W. D.; Zhao, Y. X.; Liu, Y.; Sun, M. Z.; Waterhouse, G. I. N.; Huang, B. L.; Zhang, K.; Zhang, T. R.; Lu, S. Y. Exploiting Ru-induced lattice strain in CoRu nanoalloys for robust bifunctional hydrogen production. *Angew. Chem., Int. Ed.* **2021**, *60*, 3290–3298.
[116] Li, H.; Tsai, C.; Koh, A. L.; Cai, L. L.; Contryman, A. W.; Fragapane, A. H.; Zhao, J. H.; Han, H. S.; Manoharan, H. C.; Abild-Pedersen, F. et al. Activating and optimizing MoS_2 basal planes for hydrogen evolution through the formation of strained sulphur vacancies. *Nat. Mater.* **2016**, *15*, 48–53.
[117] Jiang, K.; Luo, M.; Liu, Z. X.; Peng, M.; Chen, D. C.; Lu, Y. R.; Chan, T. S.; De Groot, F. M. F.; Tan, Y. W. Rational strain engineering of single-atom ruthenium on nanoporous MoS_2 for highly efficient hydrogen evolution. *Nat. Commun.* **2021**, *12*, 1687.
[118] Balaghi, L.; Bussone, G.; Grifone, R.; Hübner, R.; Grenzer, J.; Ghorbani-Asl, M.; Krasheninnikov, A. V.; Schneider, H.; Helm, M.; Dimakis, E. Widely tunable GaAs bandgap via strain engineering in core/shell nanowires with large lattice mismatch. *Nat. Commun.* **2019**, *10*, 2793.
[119] Pedireddy, S.; Lee, H. K.; Koh, C. S. L.; Tan, J. M. R.; Tjiu, W. W.; Ling, X. Y. Nanoporous gold bowls: A kinetic approach to control open shell structures and size-tunable lattice strain for electrocatalytic applications. *Small* **2016**, *12*, 4531–4540.
[120] Ahn, G. H.; Amani, M.; Rasool, H.; Lien, D. H.; Mastandrea, J. P.; Ager III, J. W.; Dubey, M.; Chrzan, D. C.; Minor, A. M.; Javey, A. Strain-engineered growth of two-dimensional materials. *Nat. Commun.* **2017**, *8*, 608.
[121] Alinezhad, A.; Gloag, L.; Benedetti, T. M.; Cheong, S.; Webster, R. F.; Roelsgaard, M.; Iversen, B. B.; Schuhmann, W.; Gooding, J. J.; Tilley, R. D. Direct growth of highly strained Pt islands on branched Ni nanoparticles for improved hydrogen evolution reaction activity. *J. Am. Chem. Soc.* **2019**, *141*, 16202–16207.
[122] Sun, W.; Zhou, Z. H.; Zaman, W. Q.; Cao, L. M.; Yang, J. Rational manipulation of IrO_2 lattice strain on α-MnO_2 nanorods as a highly efficient water-splitting catalyst. *ACS Appl. Mater. Interfaces* **2017**, *9*, 41855–41862.